Title
Quantum critical lines,Quantum critical fan and Measurment induced transition

Author
Yu, Hui

Publication Date
2023

Peer reviewed|Thesis/dissertation

UNIVERSITY OF CALIFORNIA
Los Angeles

Quantum critical lines, Quantum critical fan and Measurement induced transition

A dissertation submitted in partial satisfaction
of the requirements for the degree
Doctor of Philosophy in Physics

by

Hui Yu

2023

ABSTRACT OF THE DISSERTATION

Quantum critical lines, Quantum critical fan and Measurement induced transition

by

Hui Yu
Doctor of Philosophy in Physics
University of California, Los Angeles, 2023
Professor Sudip Chakravarty, Chair

After a brief introduction that overviews quantum phase transitions and quantum criticality at finite temperatures, we begin Chapter 1 by introducing an exactly solved model with multiple critical lines - transverse field Ising model with added 3-spin interaction. We focus on the phase diagram and discuss several features associated with critical lines. Then we explicitly show how to calculate the spin-spin correlation function and dynamical structure factor $S(k, \omega)$ in terms of a Pfaffian. Next, we present the zero-temperature dynamical structure factor at various critical lines in the pure and disordered systems. Finally, this chapter concludes with a discussion about further research on similar models with quantum critical lines or quantum critical surfaces.

In Chapter 2, we emphasize the finite temperature behavior of the same model as in the previous chapter by first showing any necessary modifications when the temperature is nonzero. Then we illustrate the finite temperature properties of the model in various aspects. We show how specific heat is computed and its temperature dependence at several critical points. In addition, we identify several crossovers (quantum critical to quantum disordered or renormalized classical) by classifying different temperature dependencies of the correlation length and thus constructing a quantum critical fan along one of the critical lines.

In Chapter 3, we start with an introduction to show what measurement-induced entanglement transition is and its current status. Next, we discuss our model and its setup.

Topological entanglement entropy and mutual information have been calculated to construct the phase diagram. We discover the system ends in different phases by applying non-commutative measurement gates at each time step on a line of qubits. Moreover, we obtain various critical exponents through finite-size scaling.

The dissertation of Hui Yu is approved.

HongWen Jiang

Per Kraus

Yaroslav Tserkovnyak

Sudip Chakravarty, Committee Chair

University of California, Los Angeles

2023

To my family and friends

TABLE OF CONTENTS

LIST OF FIGURES

ACKNOWLEDGMENTS

First, I would like to thank my friends and family for their mental support during my doctoral. Also, many thanks to my colleague - Steve Durr, for allowing me to cooperate with him to work on many-body localization and for providing numerous suggestions in my last year's Ph.D.

Then, I would like to express my gratitude to my advisor, Sudip Chakravarty, for allowing me to join his group and for his invaluable advice, which carried me through all stages of my research. My advisor also gives me the freedom to explore a broad range of physics.

Next, I would like to thank Steve Kivelson for sparing time to have several useful discussions with me and for providing good insights into my research project.

Finally, I would like to thank my committee members Hongwen Jiang, Per Kraus, and Yaroslav Tserkovnyak for your brilliant comments and suggestions on my thesis defense.

VITA

2016	Bachelor of Science in Math and Physics (Double Major), Purdue University, West Lafayette, Indiana.
2018	M.S. (Physics), UCLA, Los Angeles, California.
2019–Present	Ph.D Candidate (Physics), UCLA, Los Angeles, California.

PUBLICATIONS

H. Yu and S. Chakravarty. *Quantum critical points, lines, and surfaces.*, Phys. Rev. B. **107**, 045124, 2023

H. Yu and S. Chakravarty. *Quantum critical fan arising from critical lines at finite temperatures*, In Preparation. 2023

Introduction

Understanding phase transition is very important since it occurs ubiquitously in nature. In everyday life, one frequently encounters transitions like solid to liquid, liquid to gas, or vice versa. These transitions are usually achieved by changing the ambient temperature or pressure. For example, turning water into ice by freezing it or into steam by heating it. These transitions are called finite temperature phase transitions. However, we are not considering these kinds of transitions in this paper.

Instead, we focus on quantum phase transitions[1]. A quantum phase transition [Her76, SGC97, Con17, Sac99, Car10] is a phase transition between different quantum phases, determined by the ground state's property, occurring only at zero temperature. It is a widely studied subject in the condensed matter community these days. These transitions often accompany a typical setting that involves a Hamiltonian $H = H_1 + gH_2$ where H_1 and H_2 are two non-commuting terms in H. By tuning the parameter g, it is possible that the system could go from an ordered phase (symmetry-breaking) to a disordered phase (symmetry-preserving) as shown in 0.1. Precisely at the boundary between two phases, we have a point with $g = g_c$, which is referred to as a quantum critical point. There are several properties associated with a quantum critical point. (1) The ground state wave function is a superposition of many states that fluctuate at all length scales. Those quantum fluctuations are governed by Heisenberg's uncertainty principle. (2) Since fluctuation happens at all length scales, the correlation length is infinite, and thus the energy gap is zero. (3) Near the critical point, the correlation length scales as $|g - g_c|^{-\nu}$ and the energy gap scales as $|g - g_c|^{z\nu}$. Here z and ν are called critical exponents of the critical point. In particular, the value z tells us whether fluctuations in the time direction behave the same as fluctuations in the spatial direction. For a Lorentz-invariant quantum critical point, we have $z = 1$.

$$\lambda_2 = -1 \tag{0.1}$$

[1]In this paper, we put emphasis on the second-order quantum phase transition

A quantum critical point (QCP) is not the only possibility in a strongly correlated electron system. With few more tuning parameters g_1,g_2,..., in the Hamiltonian H, one could have a quantum critical line (surface), which is made out of a line (surface) of quantum critical points, in the phase diagram. Along the quantum critical line (surface), critical exponents could vary from place to place.

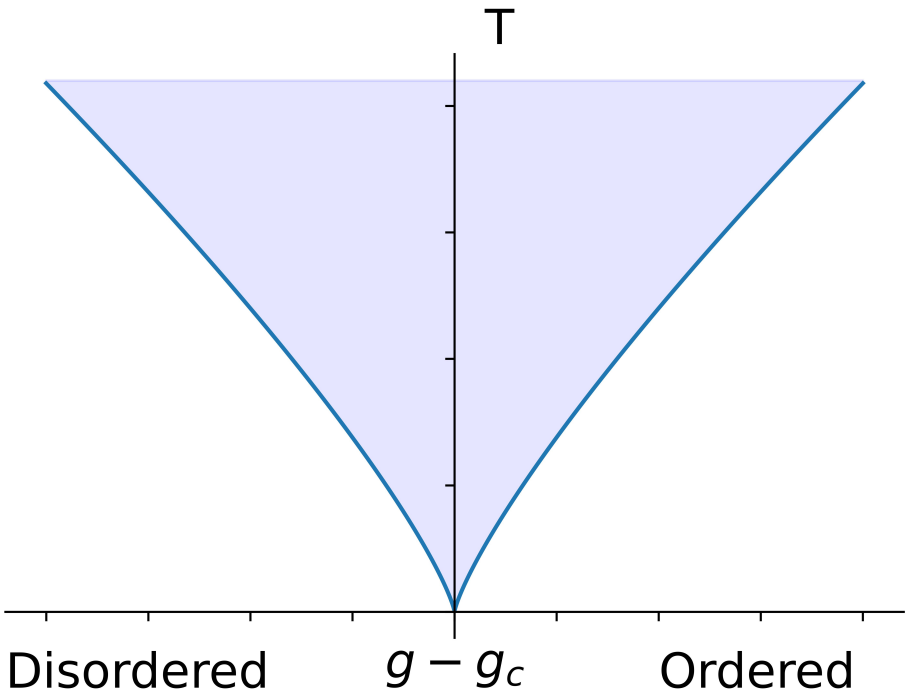

Figure 0.1: Finite temperature phase diagram for a quantum critical point g_c. At zero temperature, the system is in ordered phase for $g > g_c$ and disordered phase for $g < g_c$. The blue-shaded region is quantum critical fans. The region bounded by those lines is the regime of quantum criticality. The size or width of quantum critical fan depends on critical exponents from the critical point g_c.

Finite Temperature - Quantum Critical Fan

As mentioned before, quantum fluctuation at a critical point implies the property of the ground state. Thus, it is extremely important that one can detect these fluctuations in an experiment. Moreover, all experiments are carried out at finite temperatures. But we know quantum phase transition, by its definition, only occurs at zero temperature.

In fact, a zero temperature quantum critical point does leave fingerprints in the finite temperature phase diagram. This idea is first explored in [CHN88, CHN89] in the problem of two-dimensional quantum antiferromagnets. Finite temperature measurements reveal that the ground state has a long-ranged antiferromagnetic order [EYB88]. As shown in 0.1, the critical point g_c induces a blue-shaded region in parameter spaces as we turn on the temperature. This region is called quantum critical regime. Inside this region, one could still feel the presence or influence of those quantum fluctuations from the critical point. That extended region increases the ability to detect those fluctuations. The size or width of the critical fan depends on various exponents from the critical point. Those blue solid lines in the picture are the boundary of the critical fan. These are crossover lines determined by the relative magnitude between two energy scales in the system (temperature and energy gap). Since the energy gap is scaled as $|g - g_c|^{z\nu}$ at zero temperature, quantum criticality is obtained when the temperature is comparable to the energy gap. Thus, we have the following equation.

$$T \sim |g - g_c|^{z\nu}$$

Generally speaking, a cusp is not the only option for a quantum-critical fan. Its geometric shape relies on the exact value of those exponents.

The issue of fine-tuning

The signature of quantum criticality can now be felt in a much broad region in the phase diagram. However, this doesn't simplify experimental measurements in detecting quantum criticality. For example, a large value of $z\nu$ will make quantum critical fan narrow and thus limits the ability to detect criticality. Also, obtaining critical exponent ν in a generic strongly correlated system poses another objection to experimental measurements. All these concerns give rise to the fact quantum critical point needs to be fine-tuned. On the other hand, if zero temperature criticality is extended to a line (quantum critical line), not a point, experimental evidence of quantum criticality can be much more easily observed at finite temperatures. This is what we try to emphasize in this essay.

CHAPTER 1

Transverse field Ising model with added 3-spin interaction

This chapter is adapted from the publication:

[YC23] H. Yu and S. Chakravarty. *Quantum critical points, lines, and surfaces*, Phys. Rev. B. **107**, 045124, 2023

1.1 The Model

The one-dimensional transverse field Ising model (TFIM) is a classic example of QCP. From a theoretical point of view, the integrability of the model gives us the power to study the properties of QCP in detail. A complete discussion on that topic can be found in [Sac99]. From the experimental side, this model is well-captured by $CoNb_2O_6$ [KFM14], which illustrates the nature of quantum criticality. However, quantum critical lines are less studied in the literature. We introduce a simple but exactly solved model of a QCL. This model was introduced by Kopp and Chakravarty [KC05], with numerous exciting properties. It remains to be experimentally studied. The phase transitions in this model have intriguing topological aspects discussed by Niu [NCH12]. This model is the three-spin extension of the transverse-field Ising model. The Hamiltonian, H, is

$$H = -\sum_i (h_i \sigma_i^x + \lambda_2 \sigma_i^x \sigma_{i-1}^z \sigma_{i+1}^z + \lambda_1 \sigma_i^z \sigma_{i-1}^z) \tag{1.1}$$

written in term of standard Pauli matrices $\sigma^{x,z}$. In a pure system, we shall set $h_i = h = cst$. In disordered case, we shall let h have spatial dependence. The Hamiltonian after Jordan-Wigner [Pfe70, LSM61] transformation

$$\sigma_i^x = 1 - 2c_i^\dagger c_i \tag{1.2}$$

$$\sigma_i^z = -\prod_{j<i}(1 - 2c_j^\dagger c_j)(c_i + c_i^\dagger) \tag{1.3}$$

is

$$\begin{aligned} H = &-\sum_{i=1}^{N} h(1 - 2c_i^\dagger c_i) - \lambda_1 \sum_{i=1}^{N-1}(c_i^\dagger c_{i+1} + c_i^\dagger c_{i+1}^\dagger + h.c.) \\ &- \lambda_2 \sum_{i=2}^{N-1}(c_{i-1}^\dagger c_{i+1} + c_{i+1} c_{i-1} + h.c.). \end{aligned} \tag{1.4}$$

In contrast to the spin model, the spinless fermion Hamilitonian is actually a one-dimensional mean-field model of a p-wave superconductor, but there are both nearest- and next-nearest neighbor hopping, as well as condensates - note the pair creation $c_i^\dagger c_{i+1}^\dagger$ and destruction $c_i c_{i+1}$ operators. The solution of the corresponding spin Hamiltonian through Jordan-Wigner transformation is, however, exact and includes all possible fluctuation effects and is not a mean-field solution of any kind [Kit01].

Imposing periodic boundary conditions, a Bogoliubov transformation results in its diagonalized form:

$$H = \sum_k 2E_k \left(\eta_k^\dagger \eta_k - \frac{1}{2}\right). \tag{1.5}$$

As usual, the anticommuting fermion operators η_k's are suitable linear combinations in the momentum space of the original Jordan-Wigner fermion operators. The spectra of excitations are (lattice spacing will be set to unity throughout the paper unless stated otherwise)

$$E_k = \sqrt{1 + \lambda_1^2 + \lambda_2^2 + 2\lambda_1(1 - \lambda_2)\cos k - 2\lambda_2 \cos 2k} \tag{1.6}$$

We have set $h = 1$ when discussing the zero temperature, $T = 0$, properties. Quantum phase transitions of this model are given by the nonanalyticities of the ground state energy:

$$E_0 = -\sum_k E_k. \tag{1.7}$$

Taking the derivative of the energy dispersion, we get:

$$\frac{\partial \varepsilon_k}{\partial k} = \frac{4\lambda_2 \sin 2k - 2\lambda_1(1-\lambda_2)\sin k}{2\sqrt{2\lambda_1(1-\lambda_2)\cos k - 2\lambda_2 \cos 2k + {\lambda_1}^2 + {\lambda_2}^2 + 1}} \tag{1.8}$$

The derivative vanishes at $k = 0, \pm\pi$ and $\cos k = \lambda_1(1-\lambda_2)/4\lambda_2$. For these values of k the spectra assume minimum values. The nonanalyticites are defined by the critical lines where the energy gaps collapse.

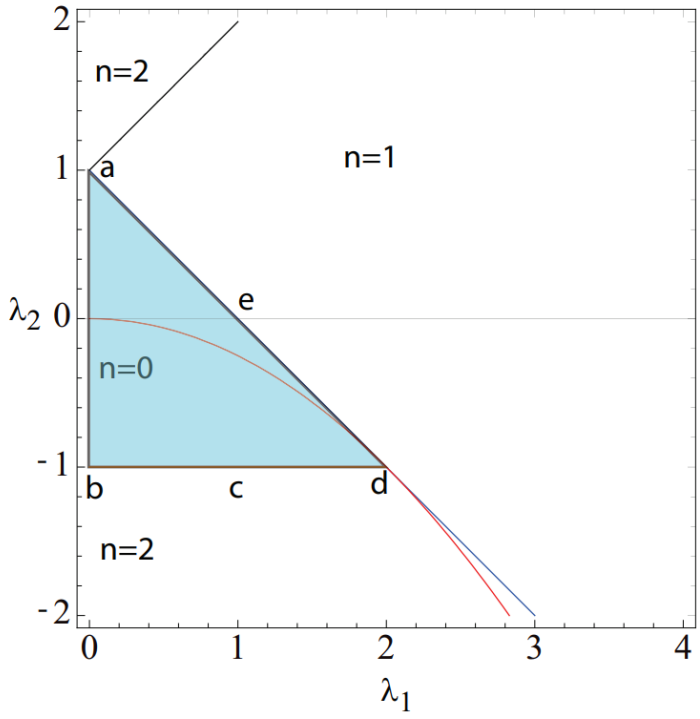

Figure 1.1: The phase diagram,$n = 0, 1, 2$, corresponds to regions with n Majorana zero modes at each other of an open chain. Three quantum critical lines ($\lambda_2 = \lambda_1 + 1, \lambda_2 = 1 - \lambda_1, \lambda_2 = -1$) are determined by the vanishing of the energy gaps. The points a and d are multicritical points. The thin red line is a disorder line of no significance to quantum criticality.

1.2 Phase diagram and several properties of the model

As we see in 1.1, we see this model has two multicritical points and three critical lines. Each critical line has different characteristics. We enumerate below some of the features of the phase diagram and its associated critical lines. To follow the description below, refer to 1.2 and 1.3:

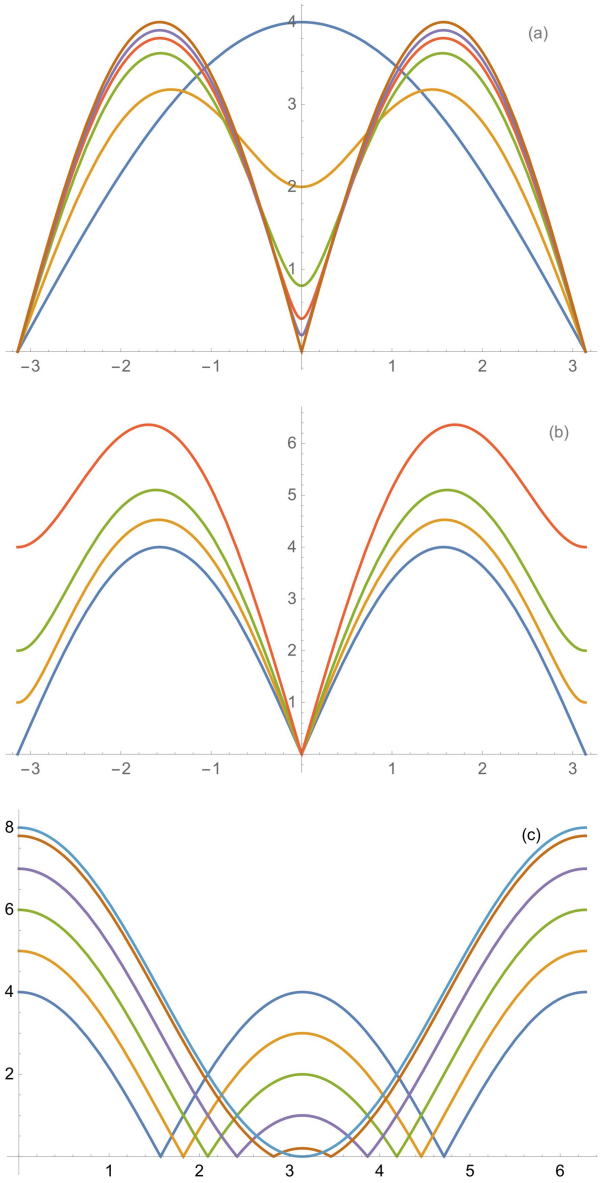

Figure 1.2: $2E_k$ vs k. The criticality along (a) $\lambda_2 = 1 - \lambda_1$: top to bottom $\lambda_1 \to 0$ (b) $\lambda_2 = 1 + \lambda_1$, where λ_1 varies between 0 and 1, and (c) $\lambda_2 = -1, 0 \leq \lambda_1 \leq 2$, plotted in the interval between 0 and 2π.

1. For the Ising model in a transverse field without a three-spin interaction, the gaps collapse at the Brillouin zone boundaries, $k = \pm\pi$ at the self-dual point $\lambda_1 = 1$ and $\lambda_2 = 0$.

2. As we move along the critical line $\lambda_2 = 1 - \lambda_1$, there are no additional critical points until we reach a multicritical point $\lambda_2 = 1$ then the gaps collapse at $k = 0$. This is shown in 1.2(a). In the language of conformal field theory, this crossover is described by Zamolodchikov's c function, which takes one from a theory of conformal charge $c = 1$ to that of charge $c = 1/2$ [NF93]. At exactly $\lambda_1 = 0$ and $\lambda_2 = 1$, we have dynamical critical exponent $z = 1$ due to the linearly vanishing spectrum at $k = 0$. Then $\lambda_2 = 1 + \lambda_1$ constitutes a critical line with criticality at $k = 0$, as we can see from 1.2(b).

3. Moreover, the gaps also collapse at $k = \cos^{-1}(\lambda_1/2)$ for $\lambda_2 = -1$ and $0 < \lambda_1 < 2$. This constitutes an unusual incommensurate critical line. Right at $\lambda_1 = 2$ and $\lambda_2 = -1$, we have a non-Lorentz invariant multicritical point with dynamical critical exponent $z = 2$. This is evident from 1.2(c) since the spectra vanish quadratically at $\pm\pi$. This fact is due to the confluence of two Dirac points.

4. In the dual representation discussed below, the region enclosed by $\lambda_1^2 = -4\lambda_2$ is an oscillatory ferromagnetically ordered phase separating from an ordered phase for $\lambda_2 < 0$, as determined by the spatial decay of the instantaneous spin-spin correlation function. This does not reflect a critical line [BM71].

5. In the spin representation, our model exhibits two phases - ordered and disordered. These phases are distinguished by the presence of long-range order. As shown in Fig 2, the long-range order is reflected in the equal-time correlation function $C(r, 0)$ from Eq (19). Both $\lambda_2 = 1 + \lambda_1$ and $\lambda_2 = 1 - \lambda_1$ separate these phases. However, the line $\lambda_2 = -1$ $(0 < \lambda_1 < 2)$ can not be understood in the usual context of quantum phase transition (symmetry breaking) since it separates two disordered phases.

6. In the fermion language, the phase transitions are best described by the number of

Majorana zero modes (n) at each end of an open chain. This view was discussed in detail in a previous paper [NCH12]. So $\lambda_2 = -1$ ($0 < \lambda_1 < 2$) is a line of topological transition that separates $n = 0$ and $n = 2$. Referring to Fig.1, the number of Majorana modes were also winding numbers [Sar18, Sar17] explained in terms of Anderson pseudospin Hamilitonian [And58], when time-reversal symmetry is preserved. More recently, the topological nature of the model was explained by the notion of a curvature renormalization group [KKR21, AMR20] that may be useful in higher-dimensional systems.

Finally, this model has a dual representation which shows that it is equivalent to an anisotropic XY-model with a magnetic field in the z-direction. It is possible that XY-version is better realized in experimental systems. Let us define the dual operators:

$$\begin{aligned} \mu_x(n) &= \sigma_z(n+1)\sigma_z(n), && (1.9)\\ \mu_z(n) &= \prod_{m\leq n} \sigma_x(m), && (1.10) \end{aligned}$$

which implies that

$$\begin{aligned} [\mu_z(n), \mu_x(n)] &= -2i\mu_y(n), && (1.11)\\ \mu_y(n) &= -i\Big(\prod_{m\leq n} \sigma_x(m)\Big)\sigma_z(n+1)\sigma_z(n). && (1.12) \end{aligned}$$

The Hamiltonian under duality transforms to

$$\begin{aligned} H_D = -\frac{2}{1+r}\sum_n \Big[&\frac{1+r}{2}\mu_x(n)\mu_x(n+1)\\ &+ \frac{1-r}{2}\mu_y(n)\mu_y(n+1) + h_z\mu_z(n))\Big], \end{aligned} \tag{1.13}$$

where we have carried out the rotations : $\mu_x(n) \to \mu_z(n)$, $\mu_z(n) \to \mu_x(n)$, $\mu_y(n) \to -\mu_y(n)$. The parameters are related by

$$\lambda_1 = \frac{2h_z}{1+r}, \ \lambda_2 = \frac{r-1}{1+r}. \tag{1.14}$$

The critical line in the XY-model, separating the disordered phase from the ordered phase, is $h_z = 1$, which corresponds to $\lambda_1 + \lambda_2 = 1$, separating the ordered phase from the disordered phase. Since the ordered and the disordered phases are exchanged under duality, the disordered phase of the three-spin model is $\lambda_1 + \lambda_2 < 1$.

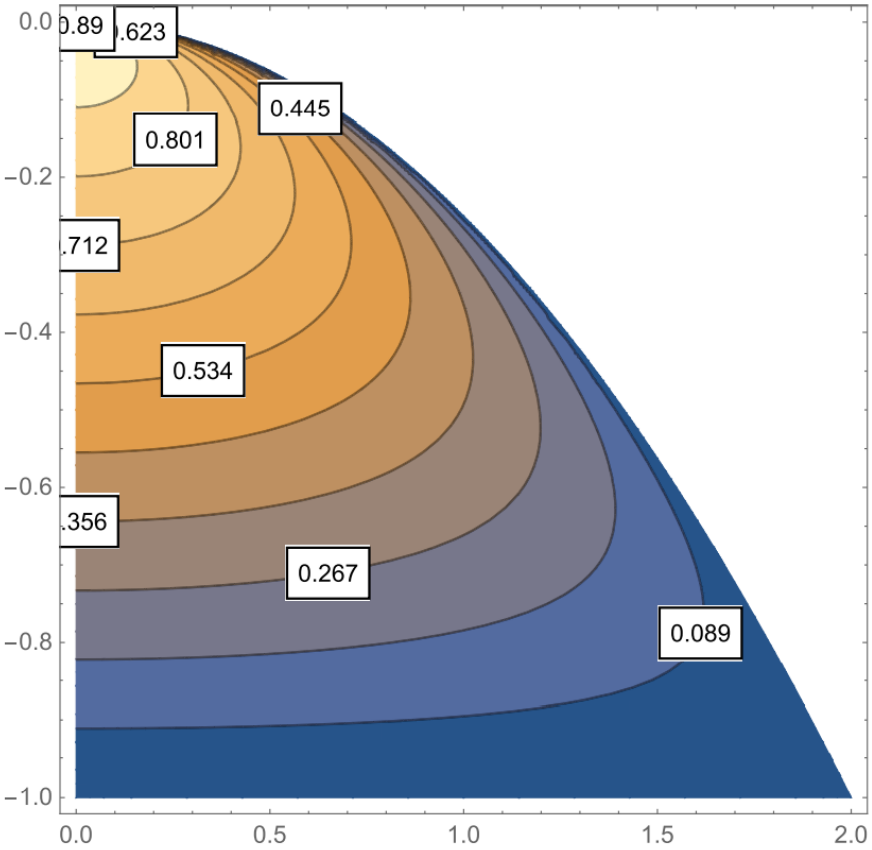

Figure 1.3: Contour plot of the square of the gap in the region $0 \leq \lambda_1 \leq 2$ and $-1 \leq \lambda_2 \leq 0$.

1.3 Correlation function in terms of a Pfaffian

In this section, we discuss the calculations in some detail. Quite generally, the spin-spin correlation function $C_{ij}(t)$ is defined as

$$C(r,t) = \left\langle \sigma_i^z(t)\sigma_j^z(0) \right\rangle \tag{1.15}$$

where i, j are lattice sites and r is the separation between them. The dynamical structure factor $S(k,\omega)$ is the time and space Fourier transformation of $C_{ij}(t) \equiv C(j-i,t) \equiv C(r,t)$. In a finite system of length L, we choose $i = [L/2 - l/2]$ to reduce the boundary effects and $j = i + l$ to compute $C(r,t)$, where $[z]$ is the largest integer smaller than z. Thus,

$$S(k,\omega) = \int dt \int dr \; e^{i\omega t} e^{-ikr} C(r,t). \tag{1.16}$$

The integral over r represents of course a discrete sum on a lattice. For the disordered case we compute

$$\overline{C}(r,t) = \overline{< \sigma_i^z(t)\sigma_j^z(0) >} \tag{1.17}$$

where the overline stands for an average over the disorder ensemble. The dynamical structure factor $S(k,\omega)$ is

$$S(k,\omega) = \int dt \int dr \; e^{i\omega t} e^{-ikr} \overline{C}(r,t) \tag{1.18}$$

Using the Jordan-Wigner transformation Eq.1.2 and 1.3. we get [LSM61]

$$C(r,t) = \left\langle \left(\prod_{m=1}^{i-1} (c_m^\dagger + c_m)(t)(c_m^\dagger - c_m)(t) \right) (c_i^\dagger + c_i)(t) \left(\prod_{l=1}^{j-1} (c_l^\dagger + c_l)(c_l^\dagger - c_l) \right) (c_j^\dagger + c_j) \right\rangle \tag{1.19}$$

Because of the free fermion nature of the Jordan-Wigner transformed Hamiltonian, we can apply Wick's theorem [Pes18] to $C(r,t)$. After collecting all terms in Wick expansion, this gives us a Pfaffian. It means that

$$\left\langle \sigma_i^z(t)\sigma_j^z \right\rangle = Pf(S) \tag{1.20}$$

Here S is a $2(i+j-1)$ dimensional skew-symmetric matrix. If we identify $A_m = c_m^\dagger + c_m$ and $B_n = c_n^\dagger - c_n$, The matrix S is

$$S = \begin{pmatrix} 0 & < A_1(t)B_1(t) > & < A_1(t)A_2(t) > & ... & < A_1(t)A_j > \\ - < A_1(t)B_1(t) > & 0 & < B_1(t)A_2(t) > & ... & < B_1(t)A_j > \\ - < A_1(t)A_2(t) > & - < B_1(t)A_2(t) > & 0 & ... & < A_2(t)A_j > \\ \vdots & \vdots & \vdots & \ddots & \vdots \\ - < A_1(t)A_j > & - < B_1(t)A_j > & - < A_2(t)A_j > & ... & 0 \end{pmatrix} \tag{1.21}$$

All we need is two-point correlation function such as

$$< (c_m^\dagger(t) \pm c_m(t))(c_l^\dagger \pm c_l) > \tag{1.22}$$

The next step is to utilize free fermion operators η_k and $\eta_k^\dagger$ to calculate the above two-point correlator. Here are the details of the remaining part of the calculation. The matrix form of the Hamiltonian in the fermion basis is

$$\hat{H} = \begin{pmatrix} c^\dagger & c \end{pmatrix} \begin{pmatrix} A & B \\ -B & -A \end{pmatrix} \begin{pmatrix} c \\ c^\dagger \end{pmatrix} \tag{1.23}$$

in which $c = (c_1, c_2 ..... c_L)$, $c^\dagger = (c_1^\dagger, c_2^\dagger ..... c_L^\dagger)$, and A and B are both $L \times L$ matrices, whose elements are

$$A_{ij} = \lambda_1(\delta_{j,i+1} + \delta_{j,i-1}) + \lambda_2(\delta_{j,i+2} + \delta_{j,i-2}) - 2h_i\delta_{ij} \tag{1.24}$$

$$B_{ij} = -\lambda_1(\delta_{j,i+1} - \delta_{j,i-1}) - \lambda_2(\delta_{j,i+2} - \delta_{j,i-2}) \tag{1.25}$$

Now, if we diagonalize H as, we get

$$\hat{H} = \begin{pmatrix} c^\dagger & c \end{pmatrix} V D V^{-1} \begin{pmatrix} c \\ c^\dagger \end{pmatrix} = \begin{pmatrix} \eta^\dagger & \eta \end{pmatrix} D \begin{pmatrix} \eta \\ \eta^\dagger \end{pmatrix} \tag{1.26}$$

Here D and V are $2L \times 2L$ matrices and take the following form.

$$D = \begin{bmatrix} E_1 & & & & & \\ & E_2 & & & & \\ & & E_3 & & & \\ & & & ... & & \\ & & & & ... & \\ & & & & & E_{2L} \end{bmatrix}, V = \begin{pmatrix} X_{L\times L} & Y_{L\times L} \\ Y_{L\times L} & X_{L\times L} \end{pmatrix} \tag{1.27}$$

$(X)_{L\times L}$ means a $L * L$ matrix. Now, our Hamilionian in the basis of η and $\eta^\dagger$ becomes

$$H = \sum_{\mu=1}^{L} 2E_\mu(\eta_\mu^\dagger \eta_\mu - 1/2) \tag{1.28}$$

We represent everything in real space since momentum representation in Eq.1.5 does not work in the disorder case; μ is no longer the momentum quantum number. The first term is the diagnolized Hamilitonian and the second term is the ground state energy. Next, in order to evaluate Eq.1.22, we need to rewrite $c^\dagger$ and c in terms of $\eta^\dagger$ and η. Since $\begin{pmatrix} c \\ c^\dagger \end{pmatrix} = V \begin{pmatrix} \eta \\ \eta^\dagger \end{pmatrix}$, we have

$$\begin{pmatrix} c^\dagger + c \\ c^\dagger - c \end{pmatrix} = \begin{pmatrix} X+Y & 0 \\ 0 & X-Y \end{pmatrix} \begin{pmatrix} \eta^\dagger + \eta \\ \eta^\dagger - \eta \end{pmatrix}. \tag{1.29}$$

Evaluation of Eq. 1.19 requires all possible m and l in Eq. 1.22. Then we can rewrite Eq. 1.22 as a $(2L\times 2L)$ matrix called C_t whose elements contain all possible two-point correlators.

$$C_t = \left\langle \begin{pmatrix} c^\dagger(t) + c(t) \\ c(t) - c^\dagger(t) \end{pmatrix} \begin{pmatrix} c^\dagger + c & c - c^\dagger \end{pmatrix} \right\rangle \tag{1.30}$$

Here $c + c^\dagger = (c_1 + c_1^\dagger, c_2 + c_2^\dagger, ..., c_L + c_L^\dagger)$. Then we use Eq.(1.29) to get

$$C_t = \begin{pmatrix} X+Y & 0 \\ 0 & X-Y \end{pmatrix} \left\langle \begin{pmatrix} \eta^\dagger(t) + \eta(t) \\ \eta(t) - \eta^\dagger(t) \end{pmatrix} \begin{pmatrix} \eta^\dagger + \eta & \eta - \eta^\dagger \end{pmatrix} \right\rangle \tag{1.31}$$

$$\begin{pmatrix} X^\dagger + Y^\dagger & 0 \\ 0 & X^\dagger - Y^\dagger \end{pmatrix}$$

Next we just need to evaluate $\left\langle \begin{pmatrix} \eta^\dagger(t) + \eta(t) \\ \eta(t) - \eta^\dagger(t) \end{pmatrix} \begin{pmatrix} \eta^\dagger + \eta & \eta - \eta^\dagger \end{pmatrix} \right\rangle$. We calculate that by first computing $\left\langle \begin{pmatrix} \eta(t) \\ \eta^\dagger(t) \end{pmatrix} \begin{pmatrix} \eta^\dagger & \eta \end{pmatrix} \right\rangle$. Here $\eta(t) = (\eta_1(t), \eta_2(t), ..., \eta_L(t))$. Fortunately, the only non-zero contraction is $\eta_i(t)$ with $\eta_j^\dagger$. It gives $< \eta_i(t)\eta_j^\dagger >= \delta_{ij}e^{i2E_it}$, Now our matrix C_t becomes

$$C_t = \begin{pmatrix} X + Y & 0 \\ 0 & X - Y \end{pmatrix} \begin{pmatrix} (\delta_{ij}e^{i2E_it})_{L\times L} & -(\delta_{ij}e^{i2E_it})_{L\times L} \\ -(\delta_{ij}e^{i2E_it})_{L\times L} & (\delta_{ij}e^{i2E_it})_{L\times L} \end{pmatrix} \begin{pmatrix} X^\dagger + Y^\dagger & 0 \\ 0 & X^\dagger - Y^\dagger \end{pmatrix} \tag{1.32}$$

Then, if one finds X and Y correctly, we are able to compute C_t without any difficulty. However, getting those eigenvectors X and Y from exact diagonalization of H is not numerically stable (suffers large errors) if their eigenvalues are very close to zero. Thus, instead of directly diagonalizing our $2L \times 2L$ Hamilitonian, we choose to use singular value decomposition (SVD) [PTV07] to diagonalize the $L \times L$ matrix. To this end, we change our basis from c and $c^\dagger$ into $c^\dagger + c$ and $c^\dagger - c$, our Hamilitonian transforms to

$$\widetilde{H} = \begin{pmatrix} c^\dagger + c & c - c^\dagger \end{pmatrix} \begin{pmatrix} 0 & M^T \\ M & 0 \end{pmatrix} \begin{pmatrix} c^\dagger + c \\ c^\dagger - c \end{pmatrix} \tag{1.33}$$

in which $M = -\frac{(A+B)}{2}$ and $M^T = -\frac{(A-B)}{2}$.

The exact form of M is

$$M = \begin{bmatrix} h_1 & -\lambda_1 & -\lambda_2 & & & \\ & h_2 & -\lambda_1 & -\lambda_2 & & \\ & & h_3 & -\lambda_1 & \ddots & \\ & & & \ddots & \ddots & -\lambda_2 \\ & & & & \ddots & -\lambda_1 \\ & & & & & h_L \end{bmatrix} \tag{1.34}$$

Next we apply SVD to matrix M. This gives us

$$M = \psi \Lambda \phi^T \tag{1.35}$$

where ψ and ϕ are $L \times L$ orthogonal matrices and Λ is diagonal with non-negative entries. This SVD also implies

$$M\phi = \psi\Lambda \tag{1.36}$$

$$M^T\psi = \phi\Lambda \tag{1.37}$$

Those are equivalent to the equation

$$\widetilde{H} \begin{pmatrix} \phi & \phi \\ \psi & -\psi \end{pmatrix} = \begin{pmatrix} \phi & \phi \\ \psi & -\psi \end{pmatrix} \begin{pmatrix} \Lambda & 0 \\ 0 & -\Lambda \end{pmatrix} \tag{1.38}$$

Then one can show the equivalence between $X + Y$, $X - Y$ and ϕ, ψ in SVD. We have

$$\begin{pmatrix} \phi & 0 \\ 0 & \psi \end{pmatrix} = \begin{pmatrix} X+Y & 0 \\ 0 & X-Y \end{pmatrix} \tag{1.39}$$

Finally, our two-point fermion-fermion correlation function becomes

$$C_t = \begin{pmatrix} \phi & 0 \\ 0 & \psi \end{pmatrix} \begin{pmatrix} (\delta_{ij}e^{i2E_it})_{L\times L} & -(\delta_{ij}e^{i2E_it})_{L\times L} \\ -(\delta_{ij}e^{i2E_it})_{L\times L} & (\delta_{ij}e^{i2E_it})_{L\times L} \end{pmatrix} \begin{pmatrix} \phi^\dagger & 0 \\ 0 & \psi^\dagger \end{pmatrix} \tag{1.40}$$

Now we can get all elements in matrix S by mapping to all elements in C_t. But we still need to deal with one last issue. The computation of a Pfaffian consumes a lot of time by standard methods for a large-sized system. An efficient method for calculating such Pfaffians was invented in a previous paper [JC06]. Let X be a $2N \times 2N$ skew-symmetric matrix which has the following form

$$X = \begin{bmatrix} A & B \\ -B^T & C \end{bmatrix} \tag{1.41}$$

where A is a 2×2 matrix, and B and C are matrices of appropriate dimensions.Then we have the identity

$$\begin{bmatrix} I_2 & 0 \\ B^T A^{-1} & I_{2N-2} \end{bmatrix} X \begin{bmatrix} I_2 & -A^{-1}B \\ 0 & I_{2N-2} \end{bmatrix} = \begin{bmatrix} A & 0 \\ 0 & C + B^T A^{-1} B \end{bmatrix} \tag{1.42}$$

where I_n is a $n \times n$ identity matrix, and

$$\det(X) = \det(A)\det(C + B^T A^{-1} B) \tag{1.43}$$

This gives us a iteration method. We will get a 2×2 matrix A in each iteration step, then we treat $C + B^T A^{-1} B$ to be our next X and keep doing this. Our $det(X)$ eventually becomes a product chain of 2×2 matrices.

1.4 Dynamical structure factor

In this section, we examine both pure and disordered versions of the model at zero temperature. For this purpose we compute a spin-spin correlation function, which is possible to be determined by neutron scattering experiments. It is difficult to find a suitable experimental technique in the superconducting picture, except perhaps by scanning tunneling microscopy. But the dynamical structure factor $S(k, \omega)$ could be measured in neutron scattering experiment. It is fortunate that we can provide a numerically exact method in this respect.

For a pure system, $S(k,\omega)$ contains no more information beyond the results for the excitation spectrum, but it encourages the experimentalists to perform the neutron measurements by measuring the spin-spin correlation function. Secondly, the method of calculation of the correlation function for the pure system can be tested before we consider the more complex disordered systems. Another important point is that it is rare that one can compute the real-time correlation function. In the present problem, this is possible because we have the full exact spectrum regardless of whether or not we have a pure or disordered case.

We treat two different models of disorder: The binary and the uniform distribution. We only allow randomness to happen in the transverse field h. The binary distribution consists of a large field h_L and a small field h_S, with the probability distributions such that $P_L + P_S = 1$ where

$$h_i = \begin{cases} h_L & \text{with probability } P_L \\ h_S & \text{with probability } P_S \end{cases} \tag{1.44}$$

in this case we keep λ_1 and λ_2 spatially independent. The probability distribution $P(h)$ for the binary distribution is

$$P(h) = P_L\ \delta(h - h_L) + P_S\ \delta(h - h_S) \tag{3}$$

The uniform distribution for h is denoted by its average h_{ave} and the width h_W. It is given by

$$P(h_i) = \begin{cases} 1/h_W, & h_i \in [h_{ave} - \frac{1}{2}h_W, h_{ave} + \frac{1}{2}h_W] \\ 0, & \text{otherwise.} \end{cases} \tag{1.45}$$

1.4.1 Pure system

The calculations in this section were performed on a chain that has 256 lattice sites with free boundary conditions. We always choose 128 sites in the middle to compute the correlation function. In the pure model, we focus on how dynamical structure factor $S(k,\omega)$ evolves

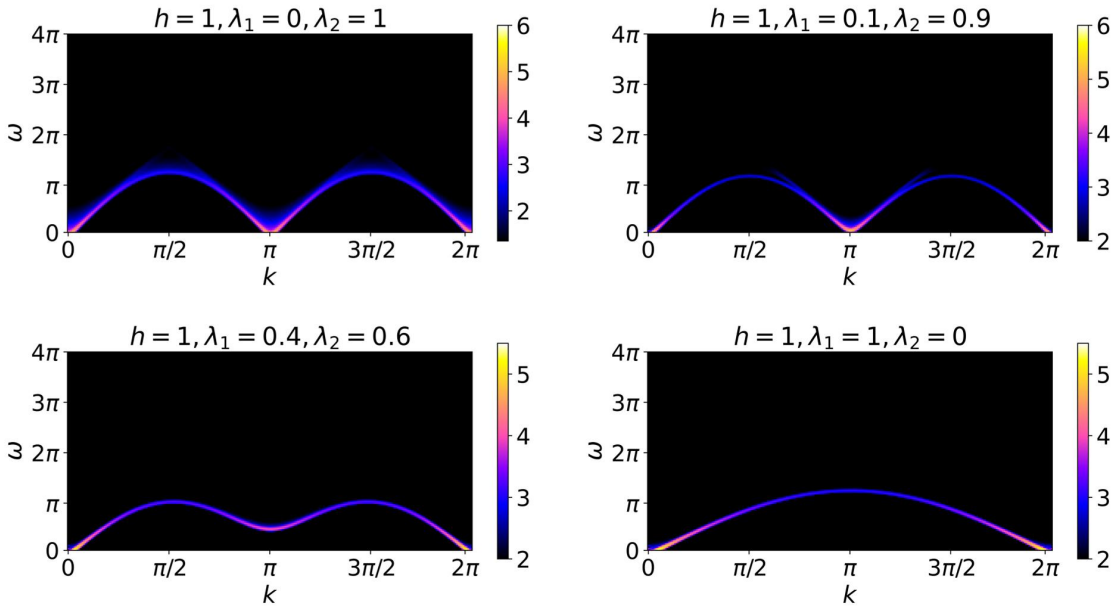

Figure 1.4: Dynamical structure factor $S(k, \omega)$ calculated at 4 points along the critical line $\lambda_2 = 1 - \lambda_1$. Top left: $\lambda_1 = 0, \lambda_2 = 1$, Top right: $\lambda_1 = 0.1, \lambda_2 = 0.9$, Bottom left: $\lambda_1 = 0.4, \lambda_2 = 0.6$, Bottom right: $\lambda_1 = 1, \lambda_2 = 0$.

along the line $\lambda_2 = 1 - \lambda_1$ as represented in 1.4. As we see in 1.4, we plot $S(k, \omega)$ at four different points, including two critical points in that region. One can see that we have exactly two modes $k = 0$ and $k = \pi$ close to $\omega = 0$. As we move to $\lambda_1 = 0.1$, $\lambda_2 = 0.9$, the energy near $k = \pi$ is no longer exactly zero. The weight in the middle shifts upward. As we move further to $\lambda_1 = 0.4$, $\lambda_2 = 0.6$, the dip near $k = \pi$ becomes more and more closer to nearby tips. As we right at the other critical point, we find out that the dip in the middle eventually levels with the nearby tips to make a transition from two arcs into one arc. Finally, we have exactly one zero mode at $\lambda_1 = 1$, $\lambda_2 = 0$. The colors in these figures are closely tied to the neutron experiment. The yellow color around $\omega = 0$ and $k = 0$ means that if you shoot a neutron beam through the model, neutrons will highly likely to have a collision with zero energy and zero momentum transfer. The darker color with energy ω and momentum k means less probability. Since the availability of energy transfer between neutrons and the system should be completely determined by the spectrum of our model, the lines traced out in the figure are the dispersion relation E_k vs k. Moreover, we can learn two interesting facts from these plots. The first one is that the highest probability is always associated with the

mode with the lowest energy. This is because collisions with less energy transfer are always preferential in zero temperature. The second interesting fact to notice is that neutrons can have collision with zero energy but finite momentum transfer (like a ball bounces off the wall) due to the appearance of zero mode $k = \pi$.

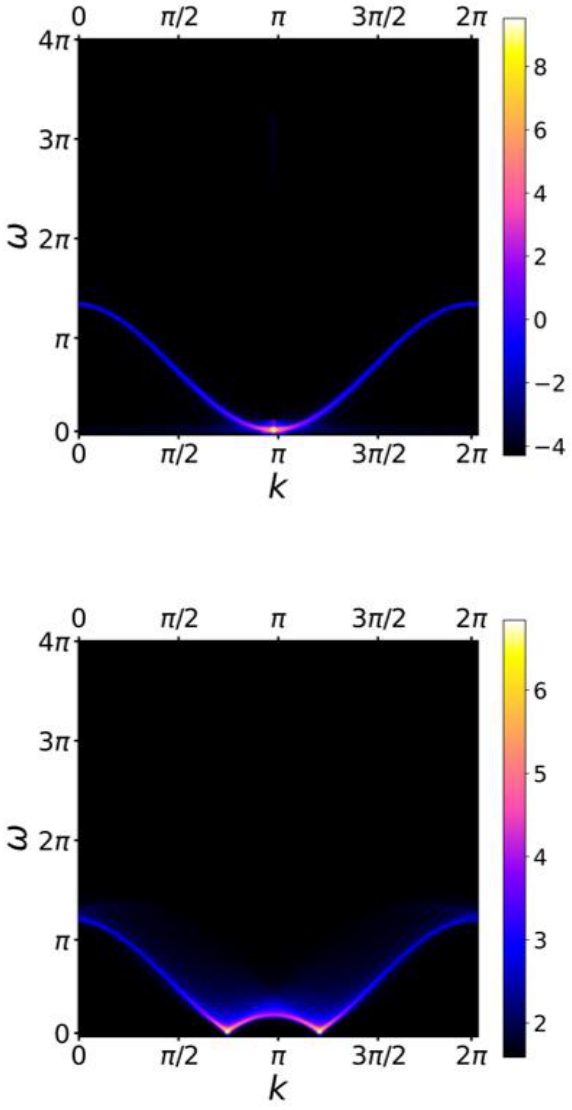

Figure 1.5: Top: The Dynamical structure factor $S(k, \omega)$ calculated at the multicritical point $\lambda_1 = 2, \lambda_2 = -1$. Bottom: $\lambda_1 = 1.5, \lambda_2 = -1$

In addition, we also plot the result as we tune λ_1 to the multicritical point $\lambda_1 = 2, \lambda_2 = -1$

along the incommensurate line (see Fig.1.5). Along the incommensurate line $\lambda_2 = -1$, we see energy gap vanishes linearly between $\pi/2$ and π and between π and $3\pi/2$. This tells us the dynamical critical exponent z is equal to one. As we move close to the multicritical point, those k values where the gap closes are also moving closer to each other. Exactly at $\lambda_1 = 2, \lambda_2 = -1$, we see the gap vanishes quadratically at $k = \pi$, this indicates z is equal to 2.

Possible neutron scattering will measure the spin-spin correlation function. It is satisfying to see that the spectra still correctly represent the fermionic excitations. It is of course not possible to directly couple to the Jordan-Wigner fermions. In addition it is a good test that our calculations are reliable and we can safely continue to the disorder problem.

1.4.2 Disordered system

A cursory look at Eq. 1.4 would seem that the disorder in this one-dimensional model will result in Anderson's localization of the fermionic states. This is not because the Hamiltonian contains pair creation and destruction operators. It corresponds to a model of a superconductor in which charge is not conserved.

The computation of $S(k, \omega)$ involves averaging of the correlation function. The calculations performed here are done averaging over 3000 realizations even though we found that there appears to be no difference between configuration averages of 1000 and 3000 samples. A representative of $S(k, \omega)$ is shown in Figs. 1.6 - 1.9. For uniform distribution, we can see disorder smears out the original spectrum. With a small value h_w (less than 1), the spectra remain intact. For a large value h_w, as we see in the bottom of 1.6, the spectra show significant broadening. For binary distribution, the disorder has a different impact on the spectra. Referring to Fig. 1.8, we can still see a quadratic dispersion at the multicritical point with a small P_L. However, if we increase P_L to 0.5, we see the dispersion breaks up into two pieces. The upper piece ($2 \leq \omega \leq 2\pi$) with a flat band that has k between $\pi/2$ and $3\pi/2$ comes from the spectra $h_L = 3$. The bottom piece ($0 \leq \omega \leq 2$) comes from part of the spectra $h_S = 1$.

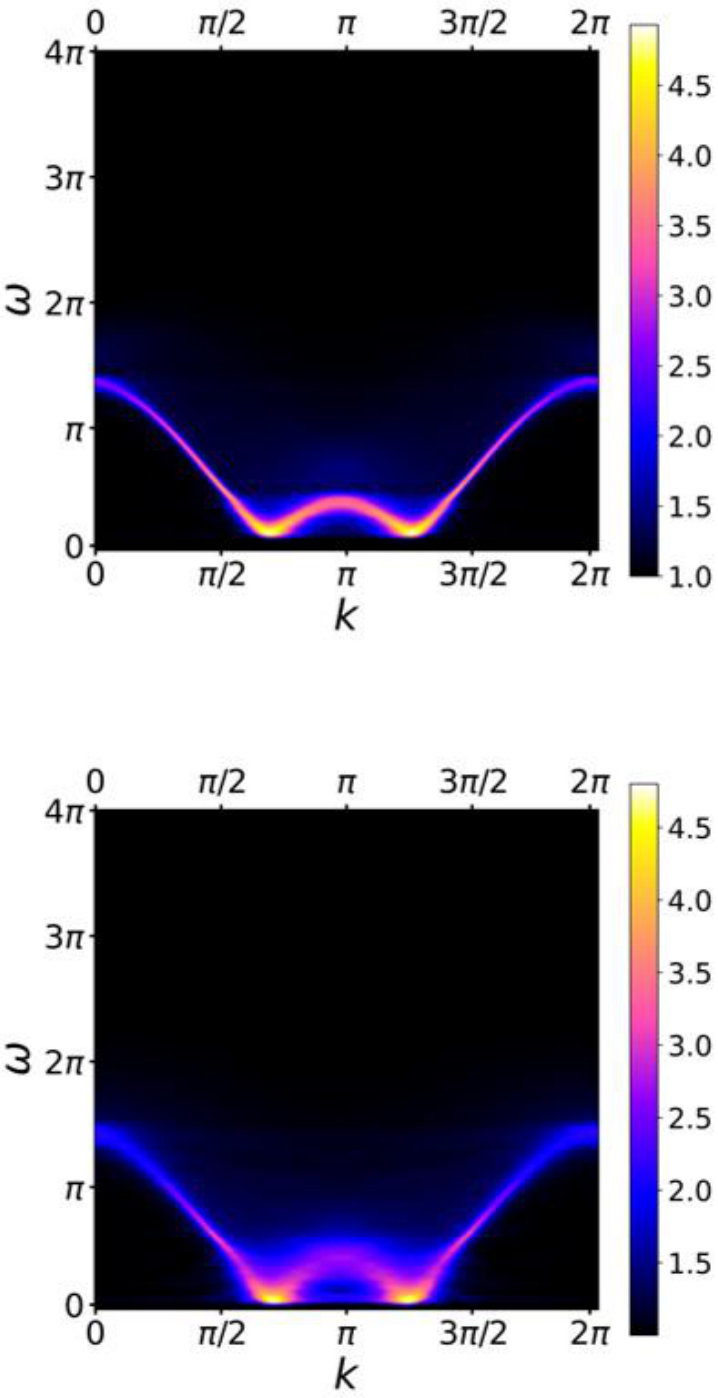

Figure 1.6: Dynamical structure factor $S(k, \omega)$ calculated for a uniform disorder. $h_{ave} = 1$. Top: $\lambda_1 = 1.5, \lambda_2 = -1$, $h_w = 1$. Bottom: $h_w = 2$

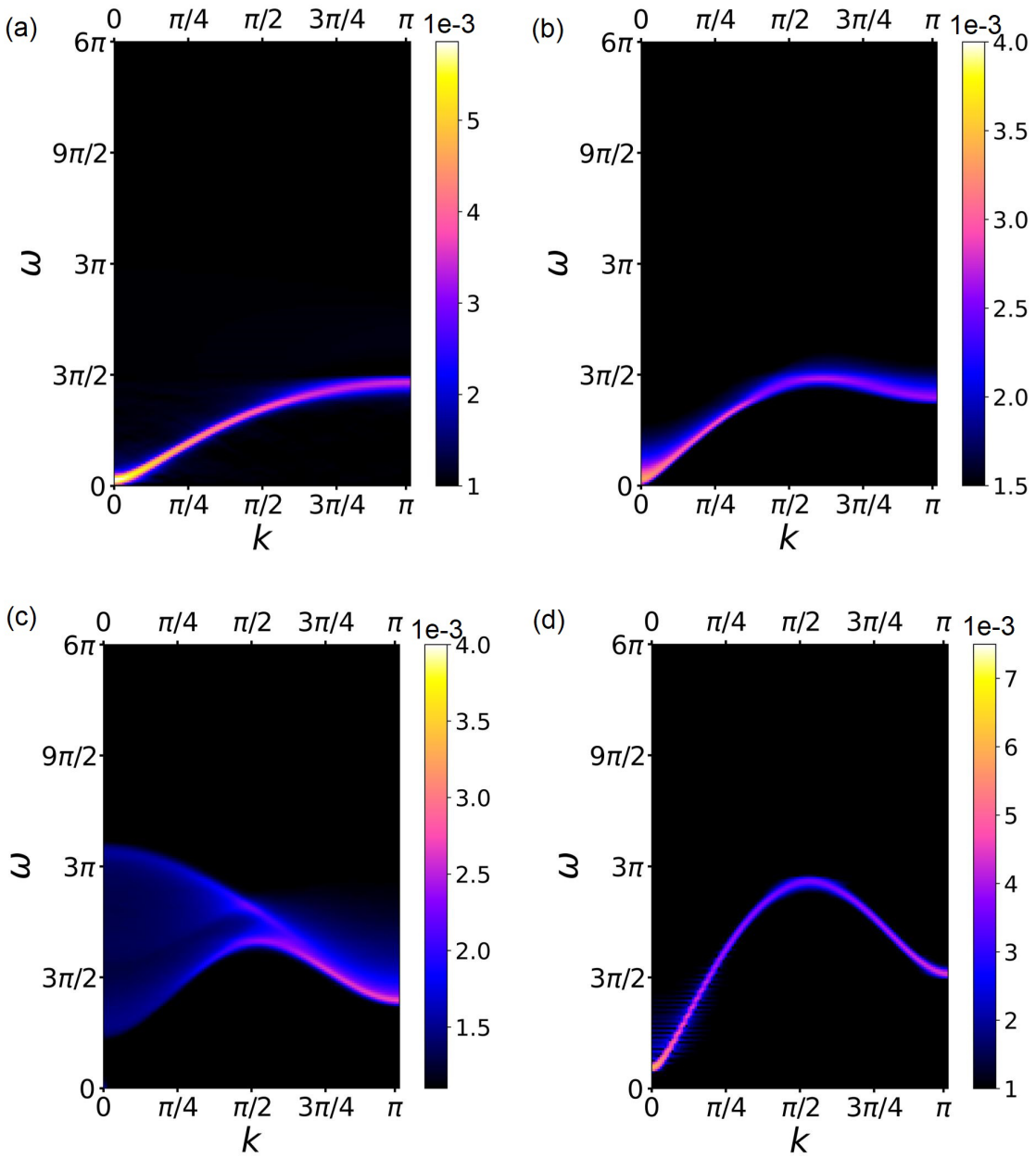

Figure 1.7: Normalized dynamical structure factor $S(k, \omega)$ with increasing value of λ_2 for uniform disorder. The parameters are $\lambda_1 = 1$, $h_{ave} = 1.4$, $h_w = 0.5$: $\lambda_2 = (a)0.1, (b)0.5, (c)1.0,$ and $(d)3.0$

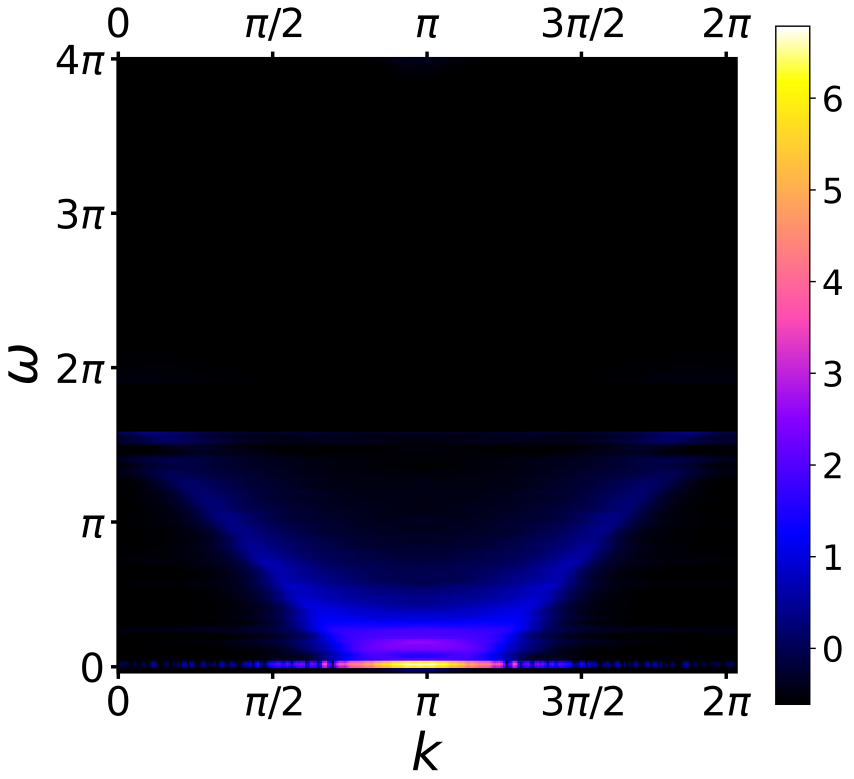

Figure 1.8: Binary distribution. The parameters are $\lambda_1 = 2$, $\lambda_2 = -1$, $h_L = 3$, $h_S = 1$, and $P_L = 0.1$ at the multicritical point. The quadratic dispersion is still visible

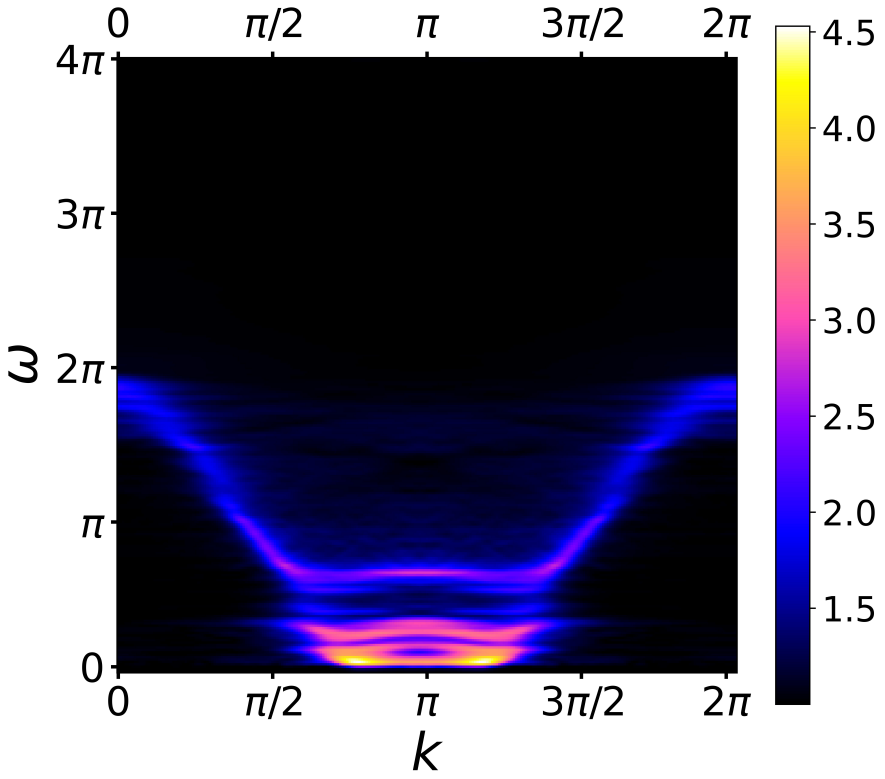

Figure 1.9: Binary distribution. The parameters are $\lambda_1 = 2$, $\lambda_2 = -1$, $h_L = 3$, $h_S = 1$, and $P_L = 0.5$ at the multicritical point. The dispersion is broken up for large disorder.

1.5 Discussion and Summary

In this chapter, we have explored an exactly solved model that exhibits three interesting quantum critical lines and two multicritical points. The centerpiece is the notion that the existence of quantum critical lines allows one to explore zero-temperature quantum critical fluctuations without excessive fine-tuning, as would be the case for a quantum critical point. The three lines have their unique characteristics. On one line, criticality is unchanged and is located at $k = \pm\pi$ with critical exponents $\nu = 1$ and $z = 1$,in the other it is centered at $k = 0$ that has the same exponents, and in the third, the criticality is at incommensurate k points. It is remarkable that the same model can exhibit such varied behavior. In addition, there are two multicritical points. One of which corresponds to nonrelativistic quadratic dispersion with a dynamical exponent $z = 2$ and a critical exponent $\nu = 1/2$.

The transition lines at $T = 0$ are topological in the sense that the number of Majorana zero modes at each end of the chain changes across the transition lines. Since all relativistic physical examples must involve some degree of disorder, we explored its effects on the dispersion spectrum. It is quite fortunate that the real-time spectra can be calculated because the model is exacly solved. Typically it is difficult to calculate the real-time spectra.

We believe that experimental realizations of the model can be found in which a free chain is all that is needed. Perhaps experimental techniques of NMR relaxation methods [KFM14] as well as terahertz spectroscopy could be employed [MAG14, CSB09]. The artifact of periodic boundary conditions is not necessary, simplifying the search for a physical model.

It is possible to extend our model by adding further neighbor interactions, still maintaining its exact solvability, so as to discuss quantum critical surfaces in the parameter space. However, the experimental realization of such models will be increasingly difficult to achieve. Finally, a QCS that is only cursorily mentioned here could be found in the language of gauge-gravity dual ideas [ZLS15].

CHAPTER 2

Finite temperature studies of TFIM with longer ranged interaction

---

This chapter is adapted from the publication:

[YC] H. Yu and S. Chakravarty. *Quantum critical fan arising from critical lines at finite temperatures*, In Preparation. 2023

2.1 Introduction

In the previous chapter, we present the result of the dynamical structure factor in the pure and disordered system at zero temperature. Here we focus on the finite temperature properties of the model. Instead, we will restrict ourselves to a pure system. We are going to show the specific heat, finite temperature $S(k, \omega)$, and the quantum critical fan from our critical lines. However, there are some subtleties we need to take care of before we dive into our studies. The Hamiltonian of TFIM with 3-spin interaction is

$$H = -\sum_i (h\sigma_i^x + \lambda_2 \sigma_i^x \sigma_{i-1}^z \sigma_{i+1}^z + \lambda_1 \sigma_i^z \sigma_{i-1}^z) \tag{2.1}$$

where we set $h = 1$ in zero temperature. At finite temperatures, we use h as a scale to measure other parameters by factoring out h from the Hamiltonian, we get

$$H = -\sum_i (\sigma_i^x + \frac{\lambda_2}{h} \sigma_i^x \sigma_{i-1}^z \sigma_{i+1}^z + \frac{\lambda_1}{h} \sigma_i^z \sigma_{i-1}^z) \tag{2.2}$$

Three critical lines $\lambda_2 = h + \lambda_1$, $\lambda_2 = h + \lambda_1$ and $\lambda_2 = -h$ becomes $\frac{\lambda_2}{h} = 1 + \frac{\lambda_1}{h}$, $\frac{\lambda_2}{h} = 1 + \frac{\lambda_1}{h}$ and $\frac{\lambda_2}{h} = -1$. In order to make the location of critical lines look the same as before, our parameters λ_1 and λ_2 are now measured in units of h. Meanwhile, the temperature T is also measured in units of h when we have the finite temperature phase diagram. The following 2.1 is the zero-temperature phase diagram labeled by the different behavior of the phases. This will be useful when we construct our finite temperature phase diagram in a later section. These ordered and disordered phases can be distinguished by the usual symmetry-breaking argument (non-zero expectation value of a local order parameter O). We show this by computing the time-independent spin-spin correlation function $C(r, 0)$. In the following sections, we start with a calculation of the correlation function and show what steps need to be modified in finite temperatures. Then we will present and discuss any results of our finite temperature study of the model.

2.2 Finite temperature correlation function

Here the finite temperature correlation function is defined as follows

$$C(r, t) = \left\langle \sigma_i^z(t)\sigma_j^z(0) \right\rangle \tag{2.3}$$

where $\sigma_i^z(t)\sigma_j^z(0)$ is no longer evaluated with respect to the ground state. The angle brackets represent a thermodynamic average $\langle(...)\rangle = Tr(e^{-\beta H}(...))/Tr(e^{-\beta H})$ in this case. The entire procedure for calculating the dynamical structure factor and time-independent correlation function is similar to what we showed before. The only modification we need to make is to recalculate all matrix elements in S from Eq. 1.21. There are four different combinations of correlators we need to consider. They are $\langle A_i(t)A_j\rangle$, $\langle A_i(t)B_j\rangle$, $\langle B_i(t)A_j\rangle$, and $\langle B_i(t)B_j\rangle$. Here is the detail for calculating $\langle A_i(t)A_j\rangle$.

$$\langle A_i(t)A_j\rangle = \left\langle (c_i^\dagger + c_j)(t)(c_i^\dagger + c_j) \right\rangle \tag{2.4}$$

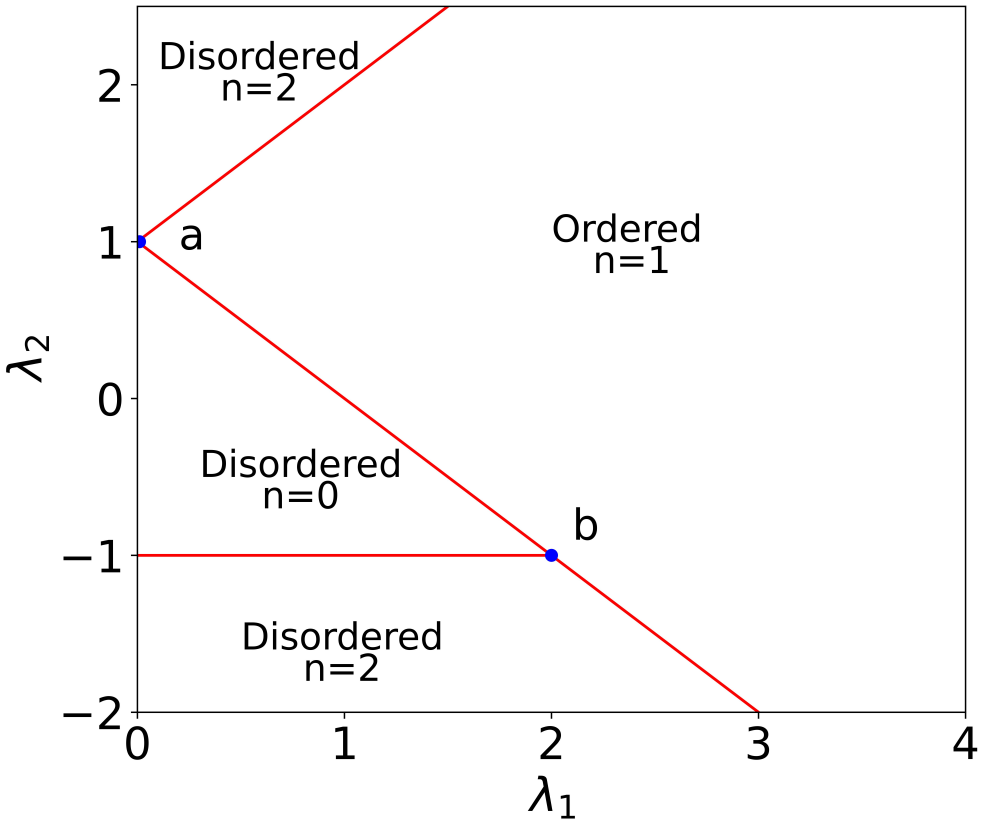

Figure 2.1: The phase diagram, n = 0,1,2, corresponds to regions with n Majorana modes at each end of an open chain. Three quantum critical lines $\lambda_2 = \lambda_1 + 1$, $\lambda_2 = 1 - \lambda_1$ and $\lambda_2 = -1 (0 < \lambda_1 < 2)$. λ_1 and λ_2 are measured in units of h. Points a and b are multicritical points with dynamical critical exponent $z = 1$ and $z = 2$. Ordered: ordered phase. Disordered: disorder phase.

Next we rewrite the correlator in η and $\eta^\dagger$ basis, we get

$$\left\langle (c_i^\dagger + c_j)(t)(c_i^\dagger + c_j) \right\rangle = \sum_{p,q=1}^{L} \phi_{pi}\phi_{qj} \left\langle (\eta_p^\dagger + \eta_p)(t)(\eta_q^\dagger + \eta_q) \right\rangle \tag{2.5}$$

Then we drop $\eta_p^\dagger \eta_q^\dagger$ and $\eta_p \eta_q$ since these terms don't conserve particle numbers. We only need to worry about the particle-conserving terms. For example,

$$\left\langle \eta_p^\dagger(t)\eta_q \right\rangle = \sum_{m,n} \left\langle m|e^{-\beta H}\eta_p^\dagger(t)|n\right\rangle \left\langle n|\eta_q|m\right\rangle / Tr(e^{-\beta H}) \tag{2.6}$$

where the sum is over single and multiparticle states and $\eta_p^\dagger(t) = e^{-iEt}\eta_p e^{iEt}$. In order to have a non-zero contribution, index p needs to be equal to q. And we compute the sum, we get

$$\left\langle \eta_p^\dagger(t)\eta_q \right\rangle = \delta_{pq}\frac{e^{-i2E_p t}}{e^{\beta 2E_p}+1} \tag{2.7}$$

where $1/e^{\beta 2E_p}+1$ comes from fermi-dirac distribution. $\left\langle \eta_p(t)\eta_q^\dagger \right\rangle$ can be computed in same manner. We get

$$\left\langle \eta_p(t)\eta_q^\dagger \right\rangle = \delta_{pq}(1-\frac{1}{e^{\beta 2E_p}+1})e^{i2E_p t} \tag{2.8}$$

Finally, we collect all terms and the result for $\langle A_i(t)A_j\rangle$ can be concretely expressed as follows

$$\langle A_i(t)A_j\rangle = \sum_{p=1}^{L}\phi_{pi}\phi_{pj}\frac{\cosh\left(2iE_p t-\beta E_p\right)}{\cosh\left(-\beta E_p\right)} \tag{2.9}$$

Similarly, one can carry out same computations for $\langle A_i(t)B_j\rangle$, $\langle B_i(t)A_j\rangle$, and $\langle B_i(t)B_j\rangle$ [DK97, You97], we have

$$\langle A_i(t)B_j\rangle = -\sum_{p=1}^{L}\phi_{pi}\psi_{pj}\frac{\sinh\left(2iE_p t-\beta E_p\right)}{\cosh\left(-\beta E_p\right)} \tag{2.10}$$

$$\langle B_i(t)A_j\rangle = \sum_{p=1}^{L}\psi_{pi}\phi_{pj}\frac{\sinh\left(2iE_p t-\beta E_p\right)}{\cosh\left(-\beta E_p\right)} \tag{2.11}$$

$$\langle B_i(t)B_j\rangle = -\sum_{p=1}^{L}\psi_{pi}\psi_{pj}\frac{\cosh\left(2iE_p t-\beta E_p\right)}{\cosh\left(-\beta E_p\right)} \tag{2.12}$$

where ϕ and ψ again come from SVD of matrix M. For time-independent correlation function , we can simplify these expressions further by setting $t=0$, we get

$$< A_i A_j >= \sum_{p=1}^{L}\phi_{pi}\phi_{pj} \tag{2.13}$$

$$< A_i B_j >= \sum_{p=1}^{L}\phi_{pi}\psi_{pj}\tanh(\beta E_p) \tag{2.14}$$

$$< B_i A_j >= -\sum_{p=1}^{L} \psi_{pi}\phi_{pj} \tanh(\beta E_p) \tag{2.15}$$

$$< B_i B_j >= -\sum_{p=1}^{L} \psi_{pi}\psi_{pj} \tag{2.16}$$

2.3 Specific Heat

This section is devoted to calculating specific heat at various points on critical lines. In order to get specific heat C, we start with the partition function Z

$$Z = \sum_{\mu} e^{-E_\mu/T} \tag{2.17}$$

where μ runs over all eigenstates, E_μ are energy for those eigenstates and T is the temperature. (Here we set $k_B = 1$) Because our model is essentially a free-fermion system after various transformations. Our partition function becomes

$$Z = \prod_{k} e^{-E_0/T}(1 + e^{-\epsilon_k/T}) \tag{2.18}$$

where $\varepsilon_k = 2\sqrt{1 + \lambda_1^2 + \lambda_2^2 + 2\lambda_1(1-\lambda_2)\cos k - 2\lambda_2 \cos 2k}$ and $E_0 = -\frac{1}{2}\sum_k \varepsilon_k$. From that, we can deduce the free energy F

$$F = -T \ln Z = \sum_{k} E_0 - T\sum_{k} \ln\left(1 + e^{-\epsilon_k/T}\right) \tag{2.19}$$

Since the first term has no T dependence, we can safely discard it. Next, we turn the discrete sum over k into a integral. We have

$$F = -TL \int_{-\pi}^{\pi} \frac{dk}{2\pi} \ln\left(1 + e^{-\epsilon_k/T}\right) \tag{2.20}$$

where L is the system's size. Finally, the expression for specific heat C is given by

$$C = -T\frac{\partial^2 F}{\partial T^2} = \frac{L}{2\pi}\int_{-\pi}^{\pi} dk\ (\frac{\epsilon_k/T}{1+e^{-\epsilon_k/T}})^2\ e^{-\epsilon_k/T}. \tag{2.21}$$

At extremely low temperatures, one can perform a calculation similar to phonons to get the exact temperature dependence of heat capacity. Here we choose a critical point from line $\lambda_2 = 1-\lambda_1$ as an example. We linearize ϵ_k (or expand around $k=\pi$) since only modes near zero energy will contribute. We get $\epsilon_k = 2\sqrt{\lambda_1^2+4(1-\lambda_1)}\ k$. Meanwhile our integration domain in Eq.(2.21) becomes $(\pi-\epsilon,\ \pi+\epsilon)$. Here ϵ is a small fixed value. Next we define $x = \epsilon_k/T$ and our Eq.(2.21) becomes

$$\frac{LT}{2\sqrt{\lambda_1^2+4(1-\lambda_1)}\pi}\int_0^{\epsilon/T} dx\ (\frac{x}{1+e^{-x}})^2 e^{-x} = \frac{LT}{2\sqrt{\lambda_1^2+4(1-\lambda_1)}\pi}\int_0^{\epsilon/T} dx\ x^2\ d(\frac{1}{1+e^{-x}}) \tag{2.22}$$

Here we send ϵ/T to ∞ by making low T approximation and apply integration by parts. We have

$$C = \frac{LT}{2\sqrt{\lambda_1^2+4(1-\lambda_1)}\pi}[x^2(\frac{1}{1+e^{-x}}-1)\Big|_0^{\infty} - \int_0^{\infty} dx\ 2x\ (\frac{1}{1+e^{-x}}-1)] \tag{2.23}$$

Then the first term vanishes exponentially and the second term can be evaluated exactly. It gives us $-\frac{\pi^2}{6}$. Then our specific heat per length is $C = \frac{\pi T}{12\sqrt{\lambda_1^2+4(1-\lambda_1)}}$. From the above derivation, we can conclude that if the dispersion of low energy mode is linear (like $\epsilon_k = v\ k$), Then our specific heat per length is $\pi T/6v$. For line $\lambda_2 = 1-\lambda_1$, $v = 2\sqrt{\lambda_1^2+4(1-\lambda_1)}$. For line $\lambda_2 = 1+\lambda_1$, $v = 2\sqrt{4\lambda_1^2+4(1+\lambda_1)}$. For line $\lambda_2 = -1$, $v = 4\sqrt{1-\lambda_1^2/4}$. But one needs to double the value of specific heat since two distinct values of k contribute to C in this case. The exact temperature dependence of the specific heat at various critical points are shown below At $\lambda_1 = 1$, $\lambda_2 = 0$, we have $v = 2\sqrt{\lambda_1^2+4(1-\lambda_1)} = 2$ and

$$C = \pi T/6v = \pi T/12 = 0.26\ T \tag{2.24}$$

At $\lambda_1 = 1$, $\lambda_2 = -1$, we have $v = 4\sqrt{1 - \lambda_1^2/4} = 4\sqrt{0.75}$ and

$$C = 2\pi T/6v = 2\pi T/24\sqrt{0.75} = 0.3\ T \tag{2.25}$$

At $\lambda_1 = 1.5$, $\lambda_2 = 2.5$, we have $v = 2\sqrt{\lambda_1^2 + 4(1 - \lambda_1)} = 2\sqrt{19}$ and

$$C = \pi T/6v = \pi T/12\sqrt{19} = 0.06\ T \tag{2.26}$$

Right at multi-critical point $\lambda_2 = -1$,$\lambda_1 = 2$. the dispersion of low energy mode is not linear but quadratic ($\epsilon_k \propto k^2$). We need to expand ϵ_k to the second order in k and thus get $\epsilon_k = 2k^2$. Next, as we did above, we restrict our domain to $(-\epsilon, \epsilon)$ and change the integration variable. We have

$$C = \frac{L\sqrt{T}}{2\sqrt{2}\pi} \int_0^{\epsilon/T} dx\ x^{3/2} (\frac{1}{1 + e^{-x}})^2 e^{-x} \tag{2.27}$$

Then we use integration by parts and send ϵ/T to ∞. We arrive at the following expression

$$C = \frac{L\sqrt{T}}{2\sqrt{2}\pi} [x^{3/2} (\frac{1}{1 + e^{-x}} - 1)\Big|_0^{\infty} - \int_0^{\infty} dx\ \frac{3}{2} x^{1/2}\ (\frac{1}{1 + e^{-x}} - 1)] \tag{2.28}$$

The first term vanishes, and the second term in the bracket gives us 1.017. So the temperature dependence of specific heat per length at this point is $\frac{1.017\sqrt{T}}{2\sqrt{2}\pi} = 0.114\sqrt{T}$. These results match the lines in 2.2.

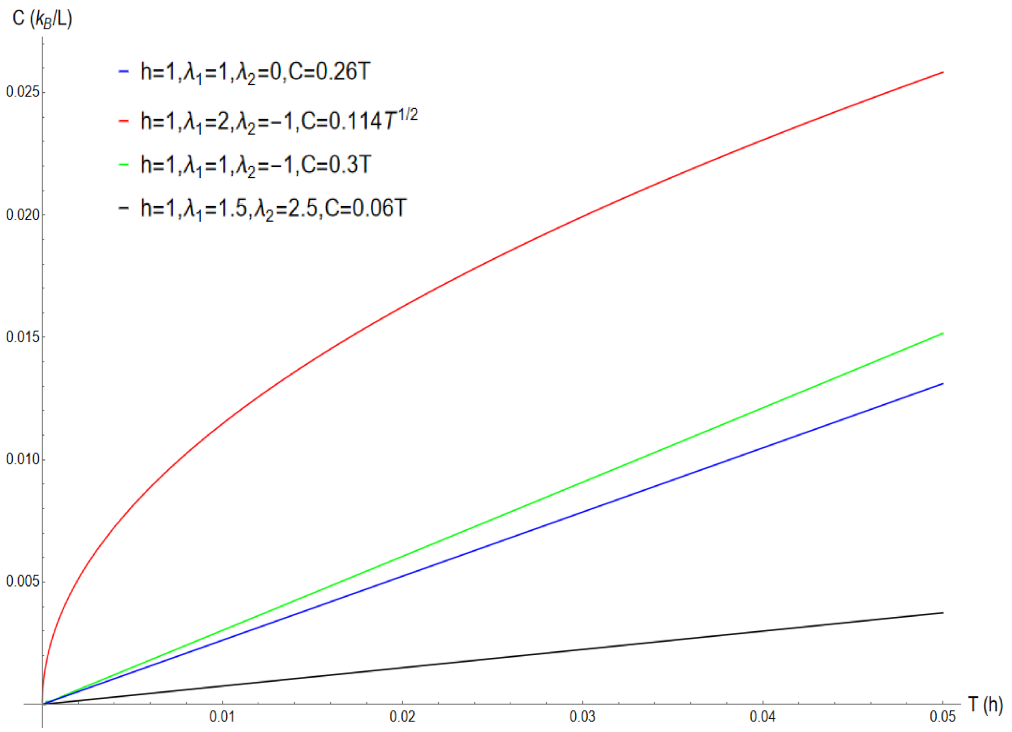

Figure 2.2: Specfic heat C calculated at various points by exact evaluation of the integral Eq. 2.21. C is measured in units of k_B/L. $z = 1$ gives you $C \sim T$ and $z = 2$ gives you $C \sim \sqrt{T}$.

2.4 Finite temperature dynamical structure factor

The previous chapter shows the dynamical structure factor $S(k, \omega)$ at zero temperature. In a pure system, $S(k, \omega)$ only contains the excitation spectrum. At finite temperatures, bogoliubov fermions η can be thermally excited. Furthermore, we need to sum over all eigenstates as Eq. 2.6 when we evaluate the spin-spin correlation function. The weight for each eigenstate is associated with the Boltzmann factor $e^{-E/T}$. These facts lead to a finite lifetime for each Bogoliubov fermion with momentum k, thus broadening the spectrum. From that, we can predict two common features from finite temperature $S(k, \omega)$. The first one is a large broadening effect corresponds to a smaller lifetime, which comes from a higher temperature (since more thermal excited particles are available to collide with). The second one is the broadening is strongest for the lowest energy in the spectra at a fixed temperature. But this broadening can not be observed at any parameters due to the competition between

energy gap Δ and temperature T. In a gapless phase (along critical lines), as shown in 2.3 and 2.4, any small temperature can immediately broaden the spectrum. We can also see the broadening becomes stronger as we increase the temperature.

However, as we move away from critical lines, we don't see any noticeable broadening within a certain temperature range. In 2.5, we see the excitation spectrum still looks the same as before. There is no significant difference between the top figure and the bottom one. Since the temperature T is smaller than the energy gap, fermions have a much lower probability of being excited. The probabilities are roughly e^{-10} for $T = 0.1$ and e^{-2} for $T = 0.5$. As we increase the temperature, fermions start to be thermally excited, and we eventually see the broadening in 2.6.

Finally, we plot a slice of $S(k, \omega)$ along fixed k at $\lambda_1 = 0.5$,$\lambda_2 = 2$. We see several interesting things in the plot. First, the location of the peak matches our expectations. If we plug the value of λ_1, λ_2 and $k = \pi$ in E_k from Eq. 1.6, we get the energy to be around 3. Second, the peak remains sharp as long as the temperature is smaller than 1. Finally, the peak does not become broaden symmetrically. As one observes more closely, one can see the peak shifts to the right, and the shape of the curve becomes more and more right-skewed. These effects are also observed in other spin chain models [JGE09, GKE10, JEK08].

2.5 Quantum critical fan

2.5.1 Ordered vs Disordered

Before we construct the finite temperature phase diagram, we need to know how our system behaves at each region separated by different critical lines in zero temperature. From 2.8, we see both $\lambda_2 = 1 + \lambda_1$ and $\lambda_2 = 1 - \lambda_1$ separate ordered phase and disordered phase. One can infer the behavior of these phases from computing time-independent correlation function $C(r, 0)$. The following description can be referred to 2.8. In the ordered phase, $C(r, 0)$ attains a finite value as r goes to ∞, which means the system possesses a long-range order. In the disordered phase, $C(r, 0)$ decays exponentially to 0 when r is around the order of $O(1)$. An

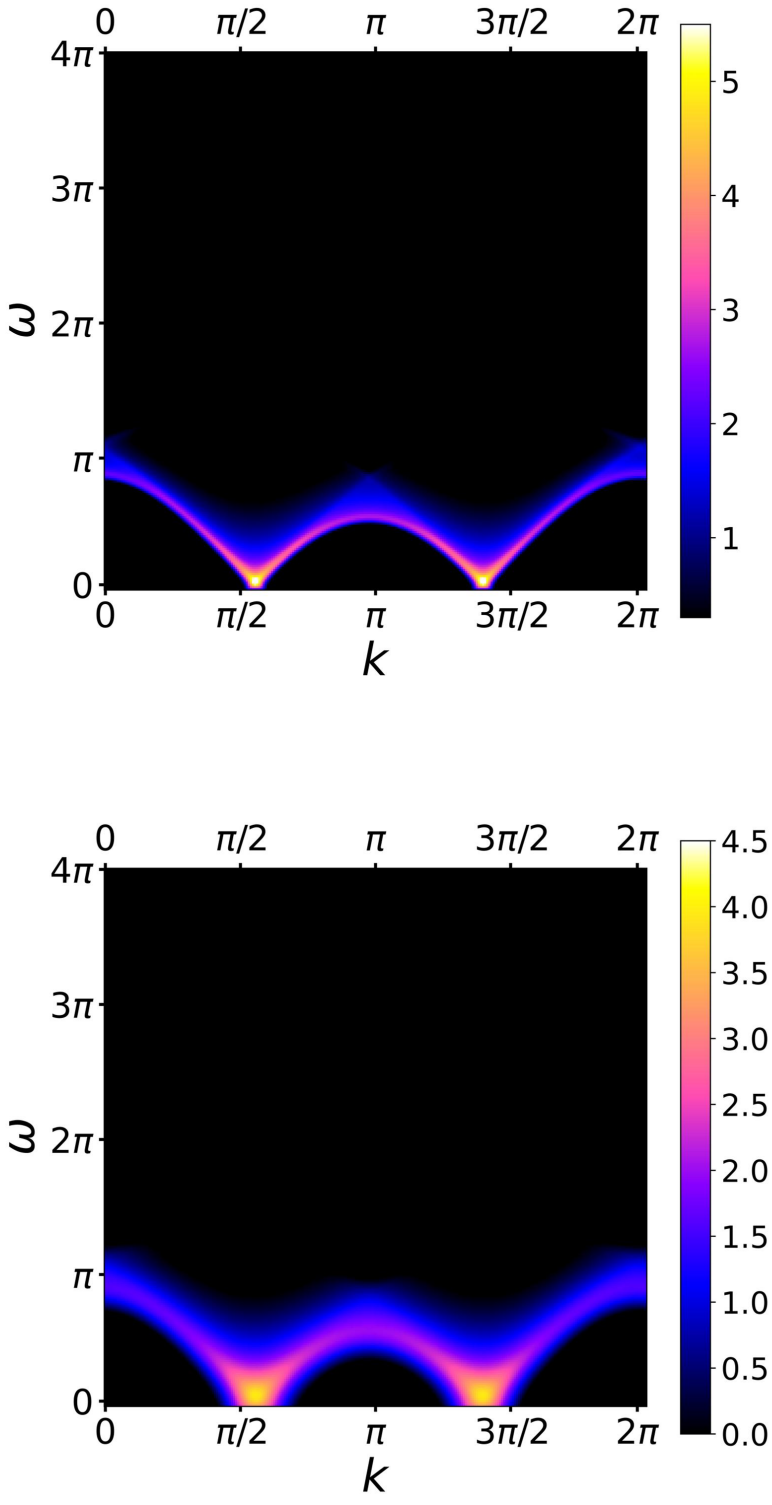

Figure 2.3: Dynamical structure factor $S(k, \omega)$ calculated at $\lambda_1 = 0.5$,$\lambda_2 = -1$ (incommensurate critical line). Top: $T = 0.01$. Bottom: $T = 0.1$.

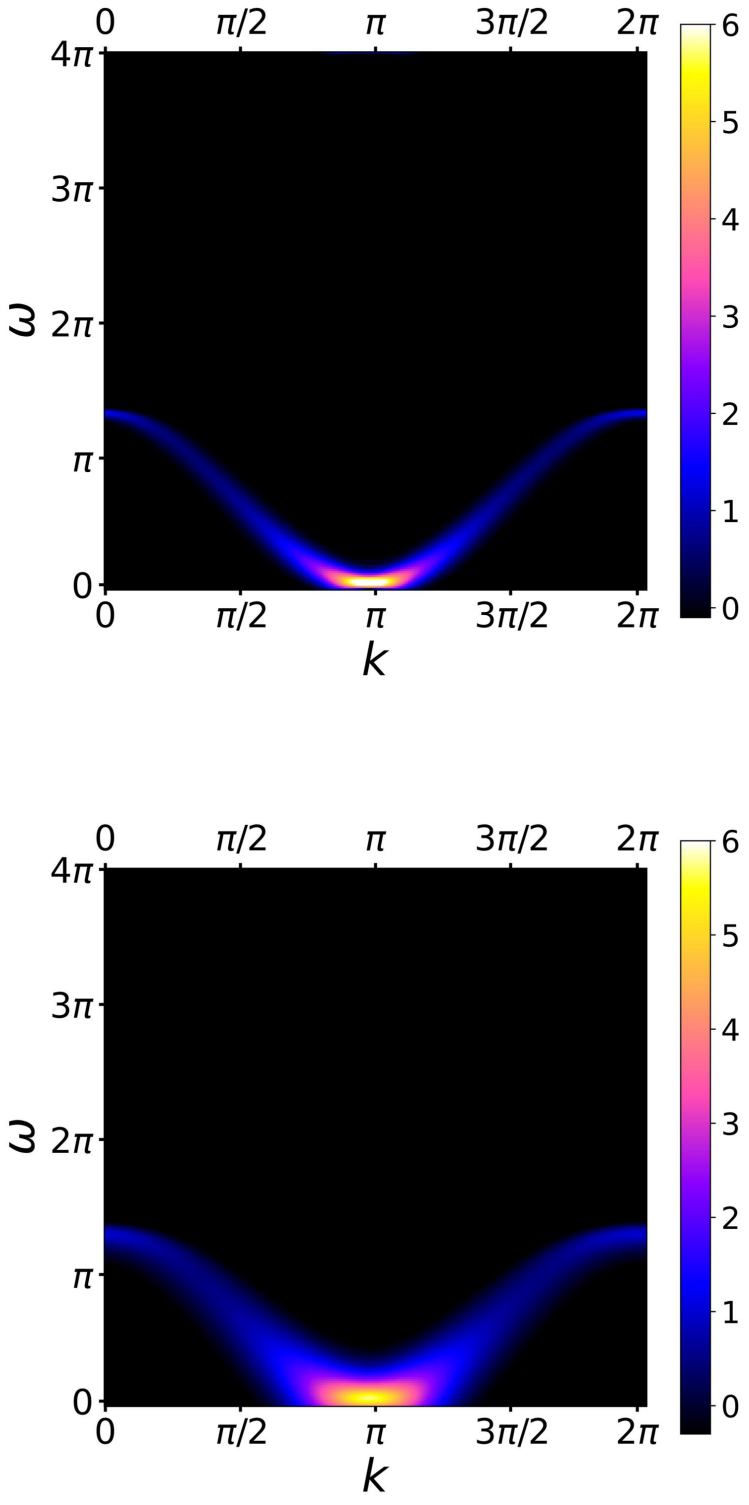

Figure 2.4: Dynamical structure factor $S(k, \omega)$ calculated at $\lambda_1 = 2$,$\lambda_2 = -1$ (multicritical point). Top: $T = 0.01$. Bottom: $T = 0.1$.

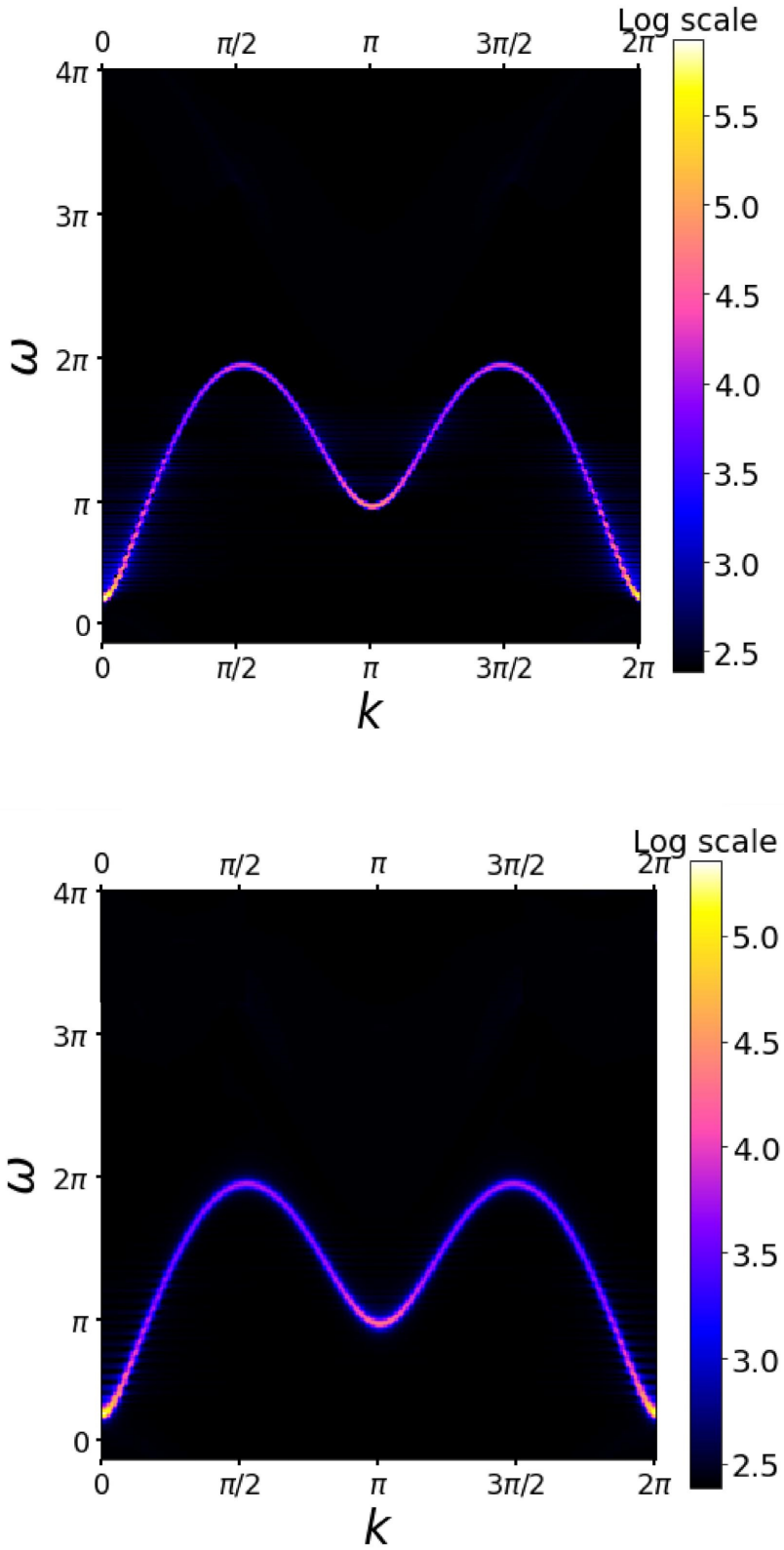

Figure 2.5: Dynamical structure factor $S(k, \omega)$ calculated at $\lambda_1 = 0.5$,$\lambda_2 = 2$ (energy gap $\Delta = 1$). Top: $T = 0.1$. Bottom: $T = 0.5$.

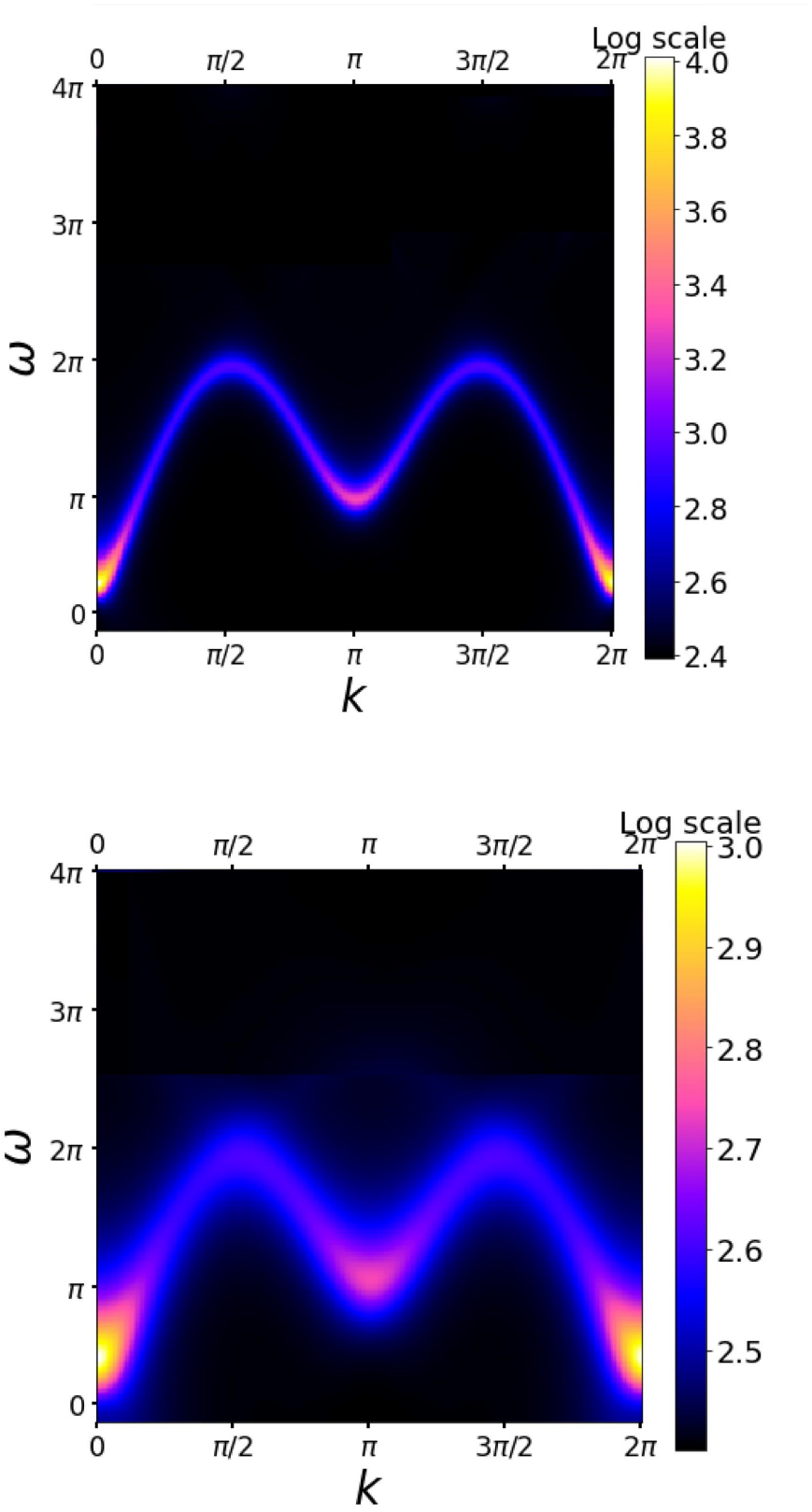

Figure 2.6: Dynamical structure factor $S(k, \omega)$ calculated at $\lambda_1 = 0.5$,$\lambda_2 = 2$ (energy gap $\Delta = 1$). Top: $T = 1$. Bottom: $T = 2$.

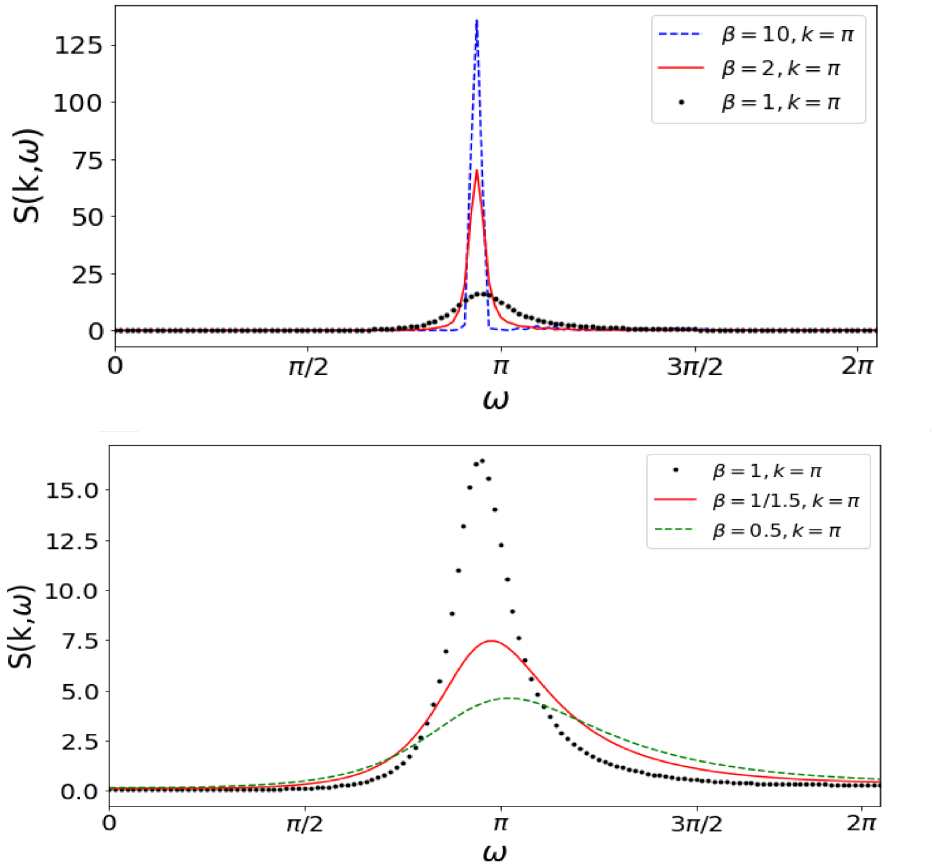

Figure 2.7: Dynamical structure factor $S(k = \pi, \omega)$ vs ω calculated at $\lambda_1 = 0.5$,$\lambda_2 = 2$. Here β is the inverse of temperature. Top: $T = 0.1$, $T = 0.5$, and $T = 1$. Bottom: $T = 1$, $T = 1.5$, and $T = 2$.

interesting fact from bottom $n = 2$ is that $C(r, 0)$ becomes negative for $1 < r < 4$. This is because that region lies below $\lambda_1^2 = -4\lambda_2$ is an oscillatory ferromagnetically ordered phase from XY model. The instantaneous spin-spin correlation from [NCH12] is $\frac{1}{x^2}e^{-2x/\xi}cos(Kx)$. The cosine function makes the correlation function oscillate between the positive and negative

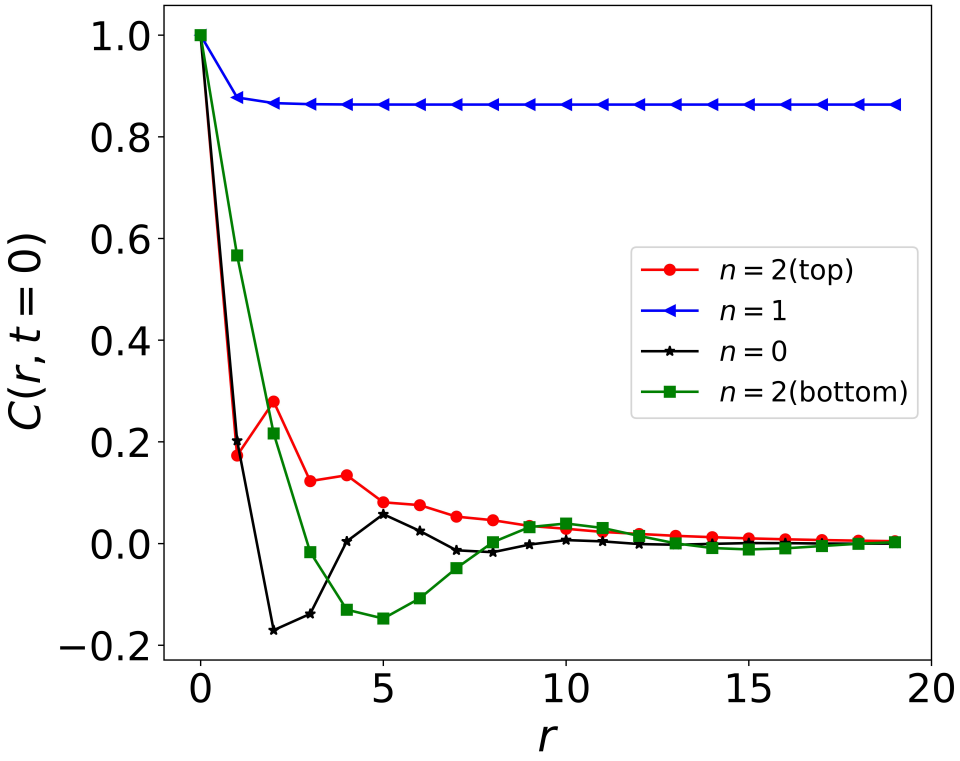

Figure 2.8: Equal-time correlation function $C(r, 0)$ at various regions which are labeled by the number of Majorana zero modes n. r is expressed in the units of lattice spacing. Red: $\lambda_1 = 0.5$, $\lambda_2 = 2$. Blue: $\lambda_1 = 1.5$, $\lambda_2 = 0$. Black: $\lambda_1 = 0.5$, $\lambda_2 = -0.5$. Green: $\lambda_1 = 2$, $\lambda_2 = -1.5$.

numbers.

2.5.2 Finite temperature phase diagram

Here we show our finite temperature phase diagram and discuss several properties of quantum critical fans and their crossovers at finite temperatures. Generically, as we raise the temperature, quantum criticality from a critical point can be felt in an extended region (quantum critical fan) in parameter space. From 0.1, the shaded region is the quantum

critical region, and its boundaries are crossover lines. The width and shape of the quantum critical fan depend on the critical exponents ν and z. In 2d parameter spaces, one can approach a critical point in any direction. This leads to a cone-like quantum critical fan for a point. In our model, with added three-spin interaction, we have a quantum critical line made from a line of critical points. Referring to 2.9, the quantum critical fan looks like a valley along the critical line in this case. Along the line $\lambda_2 = \lambda_1 - 3$, we have the usual fan diagram for a quantum critical point. These fans are crossover lines that separate different regimes (quantum critical, quantum disordered, and renormalized classical). These regimes can be distinguished by the temperature dependence of the correlation length ξ and relative magnitude between two energy scales (energy gap Δ and temperature T), as I will illustrate below.

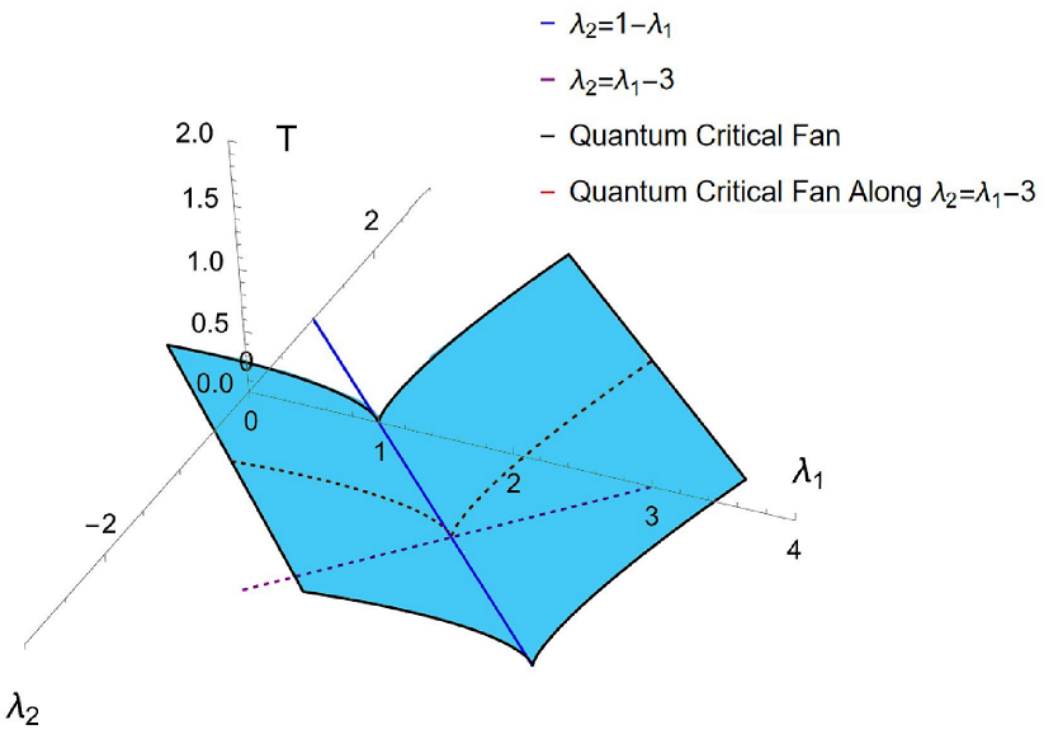

Figure 2.9: A sketch of a quantum critical fan of a quantum critical line $\lambda_2 = 1 - \lambda_1$. The blue-shaded regions are quantum critical fan. The red line is the crossover line for multicritical point $\lambda_1 = 2$,$\lambda_2 = -1$ along the direction $\lambda_2 = \lambda_1 - 3$.

2.5.2.1 Quantum Critical ($\Delta \ll T$)

In this regime, the physical properties of the model at finite temperatures are completely determined by the quantum critical point at zero temperature. There is no intrinsic scale at this point except temperature T. With the property of scale-invariance, the correlation length must behave as a power law in T.

$$\xi \sim \frac{1}{T^{1/z}} \tag{2.29}$$

where z is the dynamical critical exponent from the QCP. However, this description certainly breaks down at a certain point if the temperature is too high. One should restore the behavior of classical physics at this level. Thus, strictly speaking, one should only observe quantum criticality at $\Delta < T < max(\lambda_1, \lambda_2)$

2.5.2.2 Renormalized Classical ($\Delta \gg T$)

In this regime, ξ goes to ∞ exponentially fast as T goes to 0 due to the presence of long-range magnetic order at zero temperature. In general, we expect the correlation length to have the following form.

$$\xi \sim C_1(T) e^{C_2/T} \tag{2.30}$$

where C_2 is a constant and $C_1(T)$ is a function of T. The exact form of $C_1(T)$ is not important to us since we are only interested in the general form of ξ.

2.5.2.3 Quantum Disordered ($\Delta \gg T$)

Since there is no long-ranged order at $T = 0$, we expect the correlation length to become temperature independent as T goes to 0 and saturates to a value of order 1.

$$\xi \sim Const \tag{2.31}$$

2.5.3 Results

The calculations in this subsection are performed on a chain that has 300 lattice sites with free boundary conditions. The temperature T is measured in units of h. Full construction of quantum critical fans along our three critical lines is possible but not necessary since most quantum critical fan diagrams are quantitatively the same. Here we choose to construct the quantum fan diagrams at two points $\lambda_1 = 2$,$\lambda_2 = -1$ and $\lambda_1 = 1$,$\lambda_2 = 0$ along the direction of the line $\lambda_2 = \lambda_1 - 3$ and $\lambda_2 = \lambda_1 - 1$. The construction is based on the computation of correlation length. Generically, the equal-time correlation function $C(r, 0)$ decays exponentially at finite temperatures. This allows us to determine the correlation length ξ by fitting $C(r, 0)$ to an exponential function.

$$C(r, 0) \sim e^{-r/\xi} \tag{2.32}$$

where the prefactor could be a constant or an oscillatory function of r.

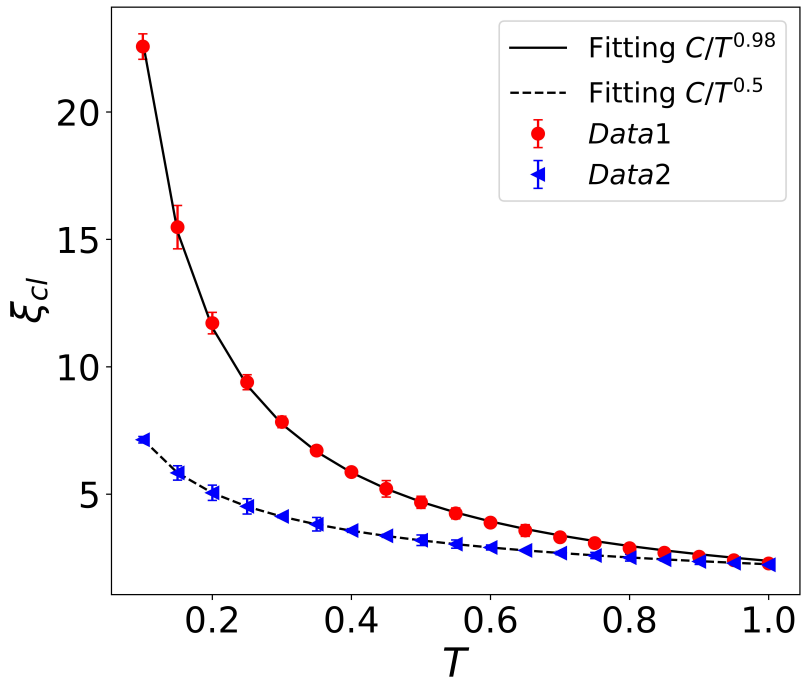

Figure 2.10: The correlation length ξ vs temperature T at two quantum critical points $\lambda_1 = 1$, $\lambda_2 = 0$ ($z = 1$) and $\lambda_1 = 2$, $\lambda_2 = -1$ ($z = 2$). $C_{top} \sim 2.38$ and $C_{bottom} \sim 2.25$.

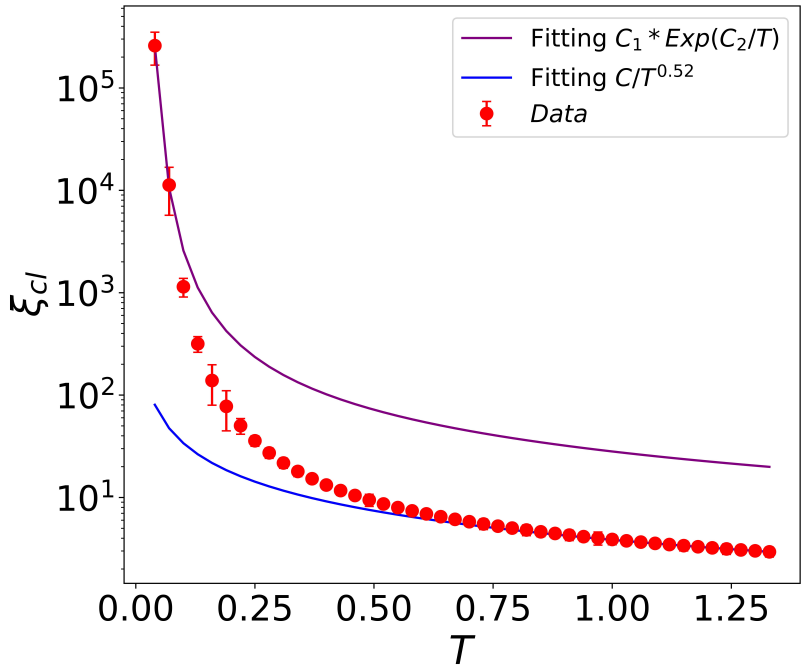

Figure 2.11: Quantum Critical to Renormalized Classical. The correlation length ξ_{CL} vs temperature T at $\lambda_1 = 2.075$, $\lambda_2 = -0.925$ ($\Delta = 0.3$). $C \sim 3.81$,$C_1 \sim 22$ and $C_2 \sim 0.25$.

2.5.3.1 Quantum Critical to Renormalized Classical

Referring to 2.10, at two multi-critical points, we see the correlation length ξ scale as $1/T^{1/z}$ with z close to the theoretical values 1(2). The coefficients C in the fitting function depend on the microscopic detail of the model, which is not our main concern. Moving away from the critical point $\lambda_1 = 2$,$\lambda_1 = -1$ into the ordered phase along the line $\lambda_2 = \lambda_1 - 3$, we see a crossover happen when we plot ξ vs T in 2.11. At high T ($T \sim 0.6$), the temperature dependence of the correlation length is almost characterized by a power law. At low T ($T \sim 0.1$), the correlation length grows exponentially to infinity due to the nature of the ordered phase. Between these regimes, we have a crossover since data points near the middle don't match any kinds of behavior mentioned. From that, we construct one side of the quantum critical fan along the lines $\lambda_2 = \lambda_1 - 3$. These are shown in 2.12. The colors in these contour plots represent the relative deviation from the power law scaling. The exact formula is

$$\log(|\xi(T) - Fit(T)|) \tag{2.33}$$

where $Fit(T)$ is the expression for the fitting function. Here we add the log function in the evaluation to minimize the difference since ξ blows up at extremely low T. The white lines are obtained by computing the energy gap at different distances to the critical point and also are expected crossover lines based on competition between the energy gap and temperature. Since we are considering crossovers, not phase transitions, we accept some misalignments between the places where the color change happens and the white lines.

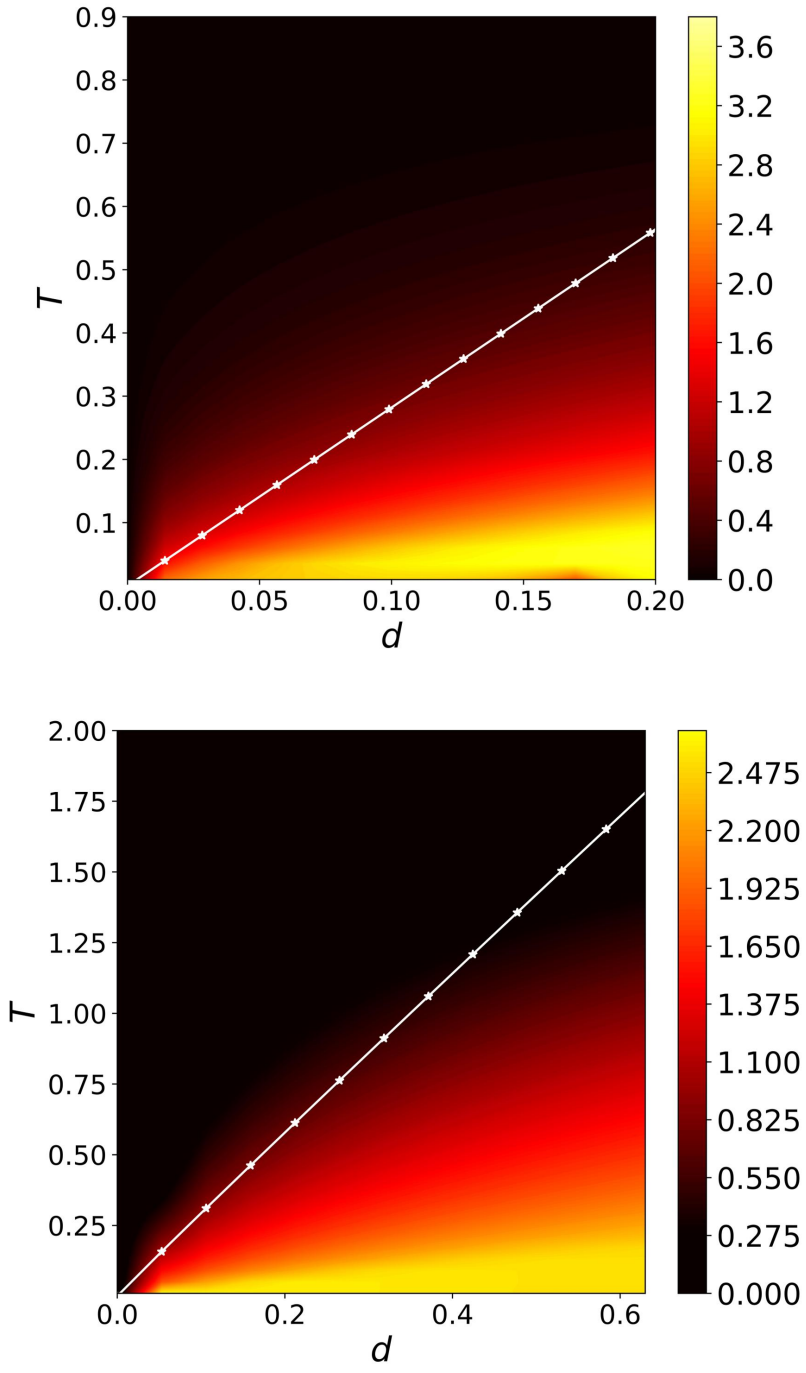

Figure 2.12: Quantum critical fan diagrams. Black: Quantum Critical. Yellow: Renormalized Classical. Top: d is the distance to the multicritical point $\lambda_1 = 1$,$\lambda_2 = 0$ ($z = 1$). Bottom: d is the distance to the multicritical point $\lambda_1 = 2$,$\lambda_2 = -1$ ($z = 2$). Two white lines are the energy gaps Δ at different d.

2.5.3.2 Quantum Critical to Quantum Disordered

Moving away from the critical point ($\lambda_1 = 2$,$\lambda_1 = -1$) into the disordered phase, we also see a crossover happen when we plot ξ vs T in 2.13. At high T ($T > \Delta$), the temperature dependence of the correlation length is again a power law. Interestingly, as we lower the temperature, we see a bump in the intermediate region ($T \sim \Delta$). But we can not differentiate whether the occurrence of the bump is due to the model itself or uncertainty from the fitting. At low T ($T < \Delta$), we see a completely different behavior. The correlation length saturates to a finite value since the nature of the ground state is disordered at zero temperature. We denote this value as ξ_{sat}, which actually depends on the distance d to the critical point.

$$\xi_{sat} \sim d^{-\nu} \tag{2.34}$$

where ν is the critical exponent. It is clear from 2.14 that ν are close to 1 ($z = 1$) and 1/2 ($z = 2$). Similarly, we construct the second half of the quantum critical fan diagrams along the lines $\lambda_2 = \lambda_1 - 1$ and $\lambda_2 = \lambda_1 - 3$. These are shown in 2.15. The colors in these contour plots again represent the relative deviations from the power law scaling. The places where color-changing happens don't perfectly match with the expected crossover line. This issue could be related to various factors - the accuracy of line fitting or the extent of validity of quantum critical fan.

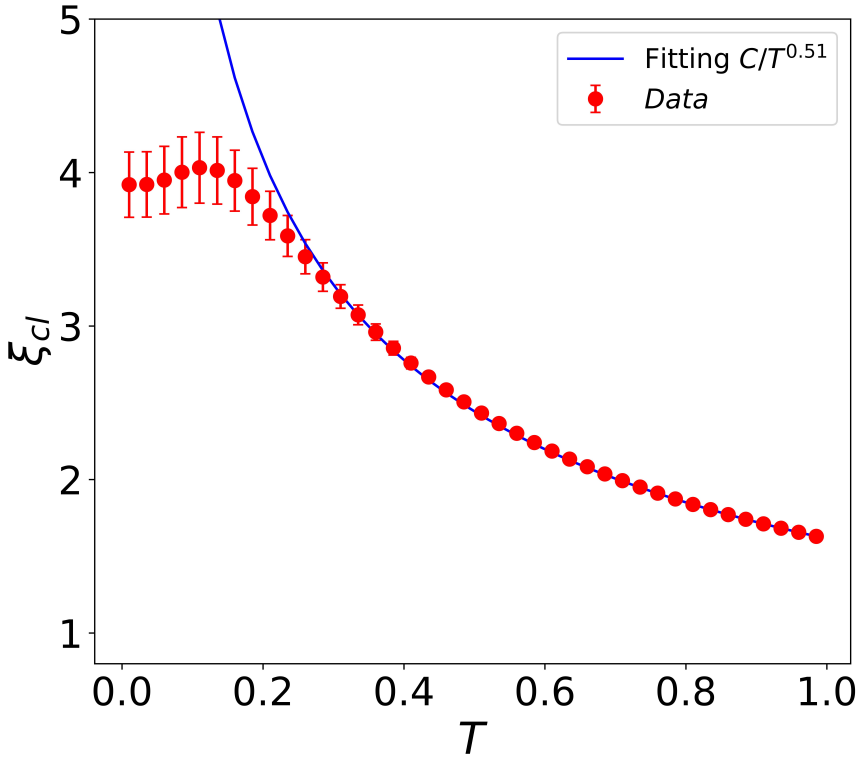

Figure 2.13: Quantum Critical to Quantum Disordered. The correlation length ξ vs temperature T at $\lambda_1 = 1.8$,$\lambda_2 = -1.2$ ($\Delta \sim 0.22$). $C \sim 1.69$

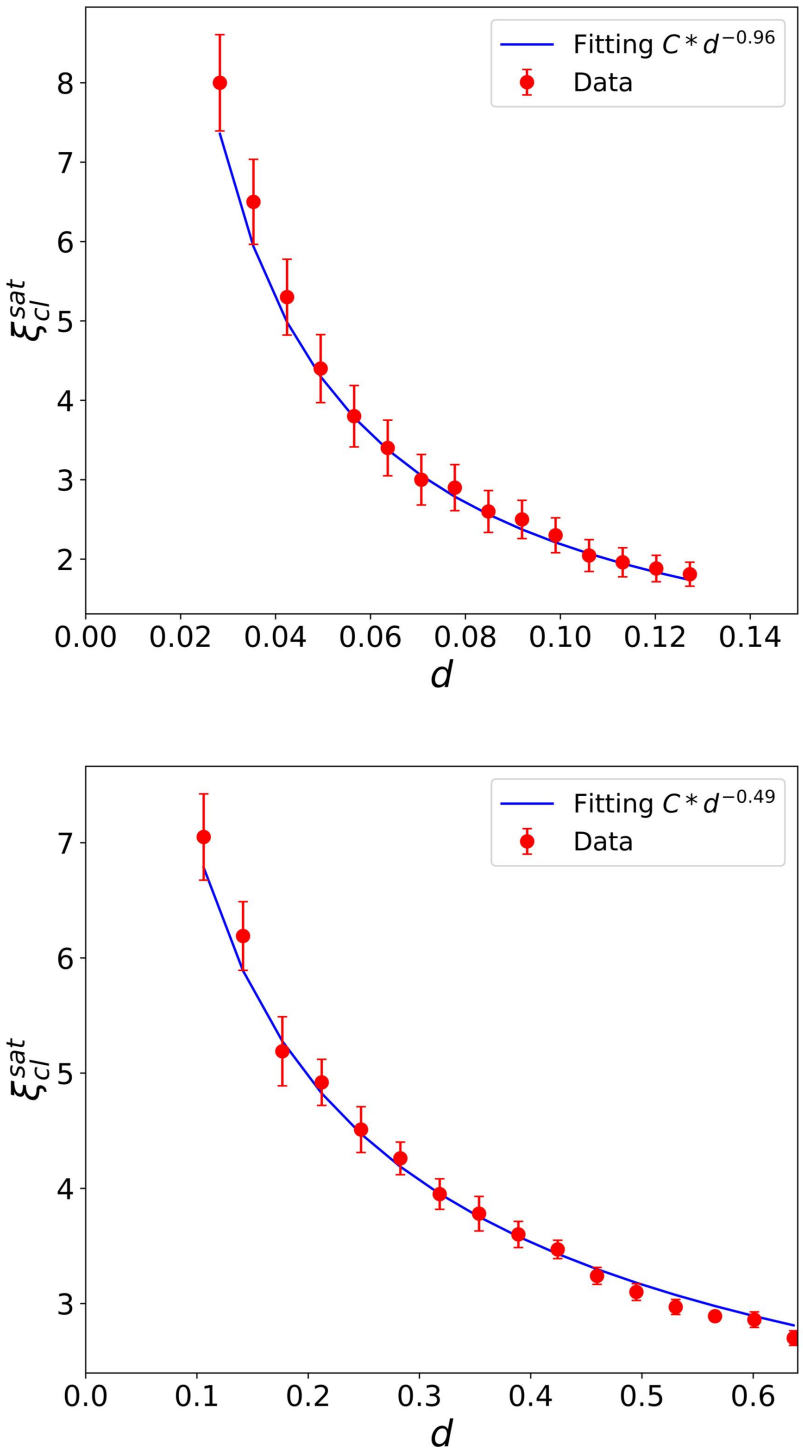

Figure 2.14: The saturated correlation length ξ_{cl}^{sat} vs distance d in quantum disordered regime. Top: d is the distance to the multicritical point $\lambda_1 = 1$,$\lambda_2 = 0$ ($z = 1$). Bottom: d is the distance to the multicritical point $\lambda_1 = 2$,$\lambda_2 = -1$ ($z = 2$). $C_{top} \sim 0.25$. $C_{bottom} \sim 2.34$

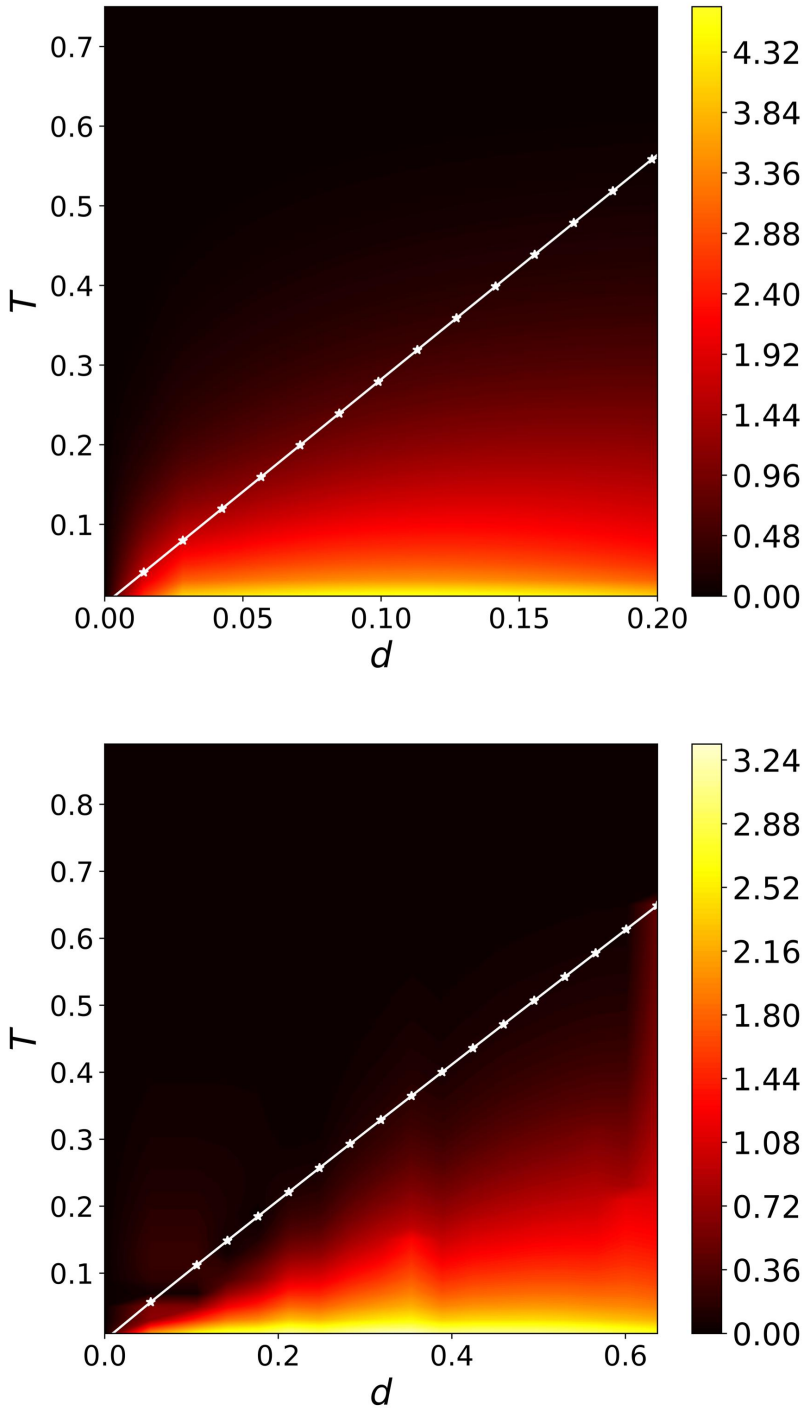

Figure 2.15: Quantum critical fan diagrams. Black: Quantum Critical. Yellow: Quantum Disordered. Top: d is the distance to the multicritical point $\lambda_1 = 1$,$\lambda_2 = 0$ ($z = 1$). Bottom: d is the distance to the multicritical point $\lambda_1 = 2$,$\lambda_2 = -1$ ($z = 2$).

CHAPTER 3

Measurement Induced Transition in a measurement-only model

3.1 Introduction

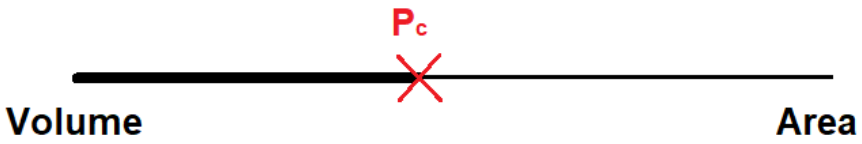

Figure 3.1: A generic phase diagram of random circuit. Unitary gates versus Measurements. Here the probability of the measurement P is the tuning parameter. The probability increases from left ($P = 0$) to right ($P = 1$). There is a phase transition between two phases at probability P_C. On the left side, the entanglement entropy satisfies a volume law. On the right side, the entanglement entropy satisfies an area law.

Out-of-equilibrium dynamics in quantum many-body systems [EFG15] have drawn much attention in recent years. New concepts and tools have been developed in these settings. Most of them come from the phenomenon of many-body localization [AP17, SPA13, HNO14], which is characterized by a breakdown of Eigenstate Thermalization Hypothesis (ETH) [Deu91, Sre94, RDO08]. Such a phenomenon is usually achieved in a closed quantum system with strong disorder. With sufficiently strong disorder, all excited states become localized. More recently, the idea of many-body effects in an open system has become popular due to the invention of noisy intermediate-scale quantum devices [Pre18]. The motivation for this direction comes from two reasons. One reason is that physicists try to understand and clas-

sify what kind of phase could emerge from an open many-body system. The other reason is that scientists can build a fault-tolerant quantum computer with the help of understanding how to control and manipulate such systems. However, a direct tackle on a generic open many-body system is difficult. Based on that, a simpler and more versatile model called random circuits has been developed [LCF18, SRN19a, LCF19, CNP19, SRS19, JYV20]. This model consists of applying unitary gates and measurements on a line of qubits. At each time step, a random unitary gate will be applied at each neighboring pair of qubits. After that, a measurement will be applied to one or multiple qubits with probability P. This iteration will continue until a steady state has been reached. Unlike conventional phase transition, the phase can only be distinguished by a non-local order parameter - Von Neumann entanglement entropy S. A generic phase diagram is depicted in 3.1. When P is near zero, measurements can not prevent the entanglement from growing. The entanglement entropy S of subsystem A is proportional to the length of the subsystem. Conversely, when P is close to one, any entanglement between two qubits built up from those random unitary gates will be killed off immediately by projective measurements. This leads to an area law for entanglement entropy S. At some intermediate value of P, we encounter a measurement-induced phase transition. Furthermore, these authors [GH20, CBQ20] explain these phases from the language of quantum error correction. In the volume-law phase, any quantum information stored in the qubits are robust against measurements. In the area-law phase, measurements will overcome the effect from the unitary gate and thus lead to the loss of information. Hence, staying in the volume-law phase becomes crucial to transmitting quantum information over a noisy channel. An experimental realization of such phase transition has been verified recently in a ion-trapped quantum computer [NNZ22].

Due to the simplicity of the model, various extensions have been made to deepen our understanding of a generic open many-body system. Several authors [LAB21, SH21, LB20, SRN19b] suggested and discovered a new class of measurement-induced transition, which is the theme of this chapter. These transitions occur in a measurement-only model. Even without unitary gates, different types of measurement gates can still lead the system to

exhibit non-trivial phases.

3.2 The Model

We start with a detailed description of our model. This model is an extension of previous work [LAB21, SH21]. Consider we have an open chain that has length L and consists of a line of qubits. All qubits are in spin-up state. Thus, our initial state $|\Psi\rangle$ is an unentangled product state. We evolve this system discretely as 3.2. At each time step, we have three options. (1) We either perform a measurement in Z direction on a single qubit with position i, which is drawn uniformly from a line of qubits, with probability P_Z. (2) Or we apply a multi-sites (two sites) measurement on a neighboring pair of qubits i, $i+1$ in X direction with probability P_{XX}. This means that suppose we get $+1$ from the measurement outcome, we discard $|+-\rangle_{i,i+1}$ and $|-+\rangle_{i,i+1}$ in the state $|\Psi\rangle$. (3) Or we apply a three-sites measurement on three qubits $i-1$, i, $i+1$ in $X_{i-1}Z_iX_{i+1}$ direction with probability P_{XZX}. If we get $+1$ from the measurement outcome, we need to discard any state that has an odd number of spin-down states in $|\Psi\rangle$. Similarly, both $(i, i+1)$ and $(i-1, i, i+1)$ from multi-site measurements are drawn independently from sets $(1,2)...(L-1,L)$ and $(1,2,3)...(L-2,L-1,L)$. We also demand this condition $P_Z + P_{XX} + P_{XZX} = 1$ to be satisfied. The type of measurement gates applied can be determined by assigning a random number P between 0 and 1 at each time step. For example, if $P < P_Z$, we choose option one above. If $P_Z < P < P_Z + P_{XX}$, we apply a X_iX_{i+1} measurement gate. Otherwise, we apply a three-sites measurement. Based on that, P_Z, P_{XX}, and P_{XZX} naturally becomes tuning parameters in our model. Certainly, at each time step, we need to renormalize $|\Psi\rangle$ after we impose a measurement gate. The renormalized state $\left|\Psi^{'}\right\rangle$ is calculated by the following

$$\left|\Psi^{'}\right\rangle = \frac{P_M \left|\Psi\right\rangle}{\sqrt{\langle P_M\Psi|P_M\Psi\rangle}} \tag{3.1}$$

where P_M is a measurement projection operator with measurement gate M. For a single site measurement, $P_Z = \frac{1\pm\sigma_i^Z}{2}$. For a two-sites measurement, $P_{XX} = \frac{1\pm\sigma_i^X\sigma_{i+1}^X}{2}$. For a three-sites

measurement, $P_{XZX} = \frac{1 \pm \sigma^X_{i-1} \sigma^Z_i \sigma^X_{i+1}}{2}$. The $\pm$ sign depends on the measurement outcome we get. Then we keep updating our state $|\Psi\rangle$ through the above iteration until an entanglement steady state is reached. It usually takes $O(Polynomial(L))$ time steps. Natively, one thinks measurements can only decrease the system's entropy by collapsing wave function. However, due to non-commutativity of different measurement gates, physical quantities related to Von Neumann entropy can grow non-trivially. This leads to an interesting phase diagram we show in later section.

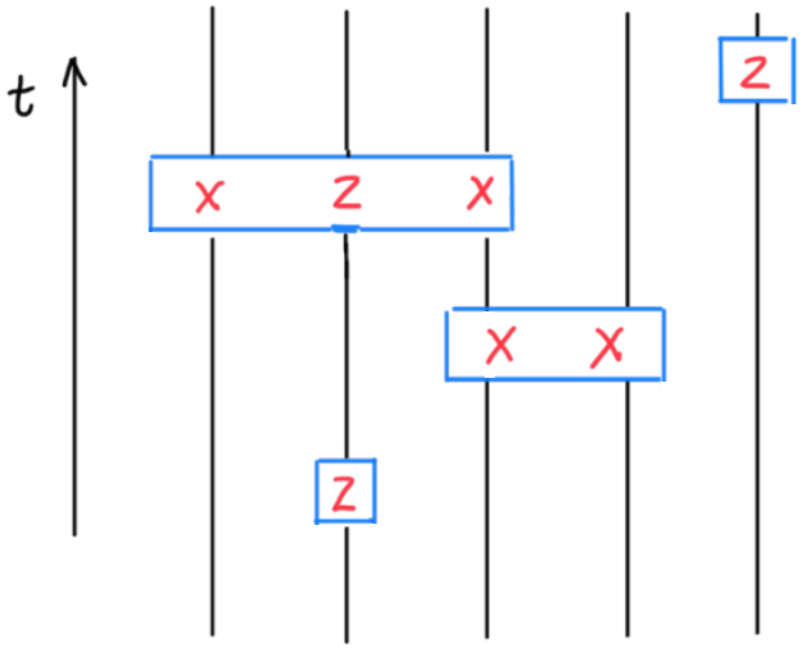

Figure 3.2: The Circuit Diagram. Five qubits ($L = 5$) in total. Time evolved discretely. Here we evolve the circuit for 4 time steps. At each time step, we apply a measurement operator (Z_i, X_iX_{i+1} and $X_{i-1}Z_iX_{i+1}$) to one qubit or multiple qubits. For example, at $t = 1$, we apply a measurement in the Z direction to the second qubit. At $t = 2$, we apply a multi-site measurement in X direction to the third and the fourth qubits.

3.3 The Method

In order to probe measurement-induced phase transition, I use two entanglement-related physical quantities to detect the transition (critical points or critical lines). One is topological entanglement entropy. The other one is mutual information. The definition of topological entanglement entropy S_{topo} is the following

$$S_{topo} = S_{AB} + S_{BC} - S_B + S_{ABC} \tag{3.2}$$

where S_{AB} stands for the Von Neumann entanglement entropy of region $A \cup B$ in the chain. $S_{AB} = -Tr(\rho_{AB} \ln(\rho_{AB}))$ and ρ_{AB} is a density matrix by tracing out all degrees of freedom from the rest of the chain ($C \cup D$). The system's partition is shown in 3.3. The chain is split into four parts with equal lengths. This physical quantity was first introduced in the context of two dimensions in [KP06]. $S_{topo} = 0$ tells us that the system is in a trivial phase. A nonzero value of S_{topo} means the system is in a topological phase and contains certain topological order (boundary modes).

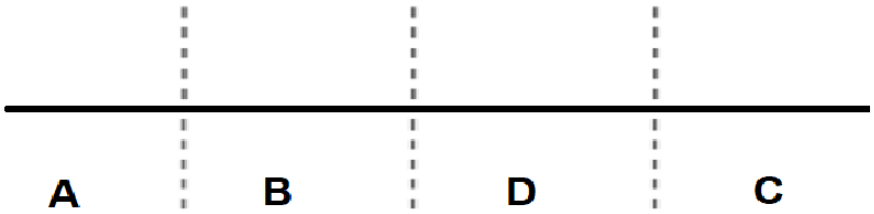

Figure 3.3: The partition of the chain for defining topological entanglement entropy S_{topo}

The definition of mutual information $I_{q_A:q_C}$ is

$$I(q_A : q_C) = S_{q_A} + S_{q_C} - S_{q_{AC}} \tag{3.3}$$

where q_A or q_C means qubits from region A or C. The mutual information $I(q_A : q_C)$ measures the entanglement between qubits in region A and qubits in region C. For example, suppose we choose one qubit from the middle of regions A and C and compute the mutual information

between these two qubits. If they are in bell state $\frac{|\uparrow\downarrow\rangle+|\downarrow\uparrow\rangle}{\sqrt{2}}$ (maximally entangled). Then the mutual information will give us 1. If they are in a product state, mutual information gives you zero. For a large size ($L > 100$) system, it is not efficient to evolve the state $|\Psi\rangle$ by storing it as a column vector as usual quantum mechanics. Since the Hilbert space for a single qubit is 2, this requires at least 2^{100} entries for the column vector. This consumes too much memory of the computer.

Here we use stabilizer formalism to encode our state $|\Psi\rangle$ and stimulate the circuit. This formalism has been used in looking at measurement-induced transitions in various circuit settings . This method was first introduced by [AG04]. For an operator O to be a stabilizer for state $|\Psi\rangle$, it has to satisfy the following property

$$O\,|\Psi\rangle = |\Psi\rangle \tag{3.4}$$

A stabilizer set for state $|\Psi\rangle$ is a set that is made up of all stabilizers for that state. Suppose we have a stabilizer set $R = \{O_1, O_2, ..., O_L\}$ for state $|\Psi\rangle$, it has to satisfy two properties

$$O_i\,|\Psi\rangle = |\Psi\rangle \tag{3.5}$$

where i goes from 1 to L

$$[O_i, O_j] = 0 \tag{3.6}$$

where i and j go from 1 to L with $i \neq j$. For example, suppose all qubits in our system are initially in $|\uparrow\rangle$ state. The stabilizer set made from all stabilizers for this state is $\{Z_1, Z_2, ..., Z_L\}$. Here we use Z or X to represent Pauli matrices σ^Z or σ^X. To represent a pure state, the number of stabilizers in the set is equal to the size of the system. A mixed state can be obtained by specifying fewer stabilizers. However, as we apply a measurement gate at each time step, our stabilizer set R needs to be updated and is not trivial. In order to implement this updating step efficiently on the computer, we represent any arbitrary operators as a binary vector. Suppose we have a Pauli string operator O acts on our circuit

and has the following form

$$O = \prod_{i=1}^{L} X_i^{m_i} \prod_{i=1}^{L} Z_i^{n_i} \tag{3.7}$$

where m_i's and n_i's are entries from two $1 \times L$ vectors $m = (m_1, ..., m_L)$ and $n = (n_1, ..., n_L)$. Thus, any Pauli string operator O can be represented as a $1 \times 2L$ vector $k_O = (m_1, ..., m_L, n_1, ..., n_L)$. We denote k_O as the binary representation of operator O. For example, as **??**, the binary representation for Z_2 at $t = 1$ is

$$k_{Z_2} = (0, 0, 0, 0, 0|0, 1, 0, 0, 0) \tag{3.8}$$

The binary representation for X_3X_4 at $t = 2$ is

$$k_{X_3X_4} = (0, 0, 1, 1, 0|0, 0, 0, 0, 0) \tag{3.9}$$

The binary representation for $X_1Z_2X_3$ at $t = 3$ is

$$k_{X_1Z_2X_3} = (1, 0, 1, 0, 0|0, 1, 0, 0, 0) \tag{3.10}$$

where we put | in the middle to distinguish X and Z operators. Given a stabilizer set R, one can build a $L \times 2L$ matrix G by taking the binary representation of elements in R as its row. For example, if all fives qubits are in the spin-up state, we have $R = \{Z_1, Z_2, ..., Z_5\}$ and its corresponding stabilizer matrix is

$$G = \begin{pmatrix} 0 & 0 & 0 & 0 & 0 & 1 & 0 & 0 & 0 & 0 \\ 0 & 0 & 0 & 0 & 0 & 0 & 1 & 0 & 0 & 0 \\ 0 & 0 & 0 & 0 & 0 & 0 & 0 & 1 & 0 & 0 \\ 0 & 0 & 0 & 0 & 0 & 0 & 0 & 0 & 1 & 0 \\ 0 & 0 & 0 & 0 & 0 & 0 & 0 & 0 & 0 & 1 \end{pmatrix} \tag{3.11}$$

For a system with length L, the stabilizer matrix G is

$$G = (0_{L\times L}|1_{L\times L}) \tag{3.12}$$

where $1_{L\times L}$ is an identity matrix with size $L \times L$. Every state $|\Psi\rangle$ has its stabilizer matrix since every state has its stabilizer set. Because of different types of measurement gates applied at each time step, the wavefunction $|\Psi\rangle$ changes. Thus we need to set up a few rules regarding How to update the stabilizer matrix G. Suppose we apply a Pauli string operator O at time t and denote the stabilizer set R at time $t-1$ as R_{t-1}.

Case 1 (Operator O commutes with every stabilizer in the set R_{t-1}): For example, a single qubit measurement in Z direction on a state that has stabilizer set $\{Z_1, Z_2, ..., Z_L\}$. In that case, applying a measurement operator O has no effect on the state $|\Psi\rangle$. Then we don't update R and thus $R_t = R_{t-1}$ ($G_t = G_{t-1}$).

Case 2 (Operator O does not commute with some stabilizers in the set R_{t-1}): For example, a two-sites measurement X_1X_2 applied on a pair of qubit does not commute with Z_1 and Z_2 in the set $\{Z_1, Z_2, ..., Z_L\}$. Based on that, we need to replace Z_1 and Z_2 from the set with new stabilzers such that these new stabilzers communte with X_1X_2 and $\{Z_3, Z_4, ..., Z_L\}$. This is accomplished by using anti-commutation relation from Pauli matrices. Suppose operator O anticommutes with stabilizers $O_1, ..., O_m$ in R_{t-1}, then we update our stabilizer set by replacing O_1 with $\pm O$ and O_i with $\pm O_1O_i$ for $i = 2, ..., m$. The choice of $\pm$ depends on the measurement outcome (± 1). Here I choose $+$ for all measurement operators O since von Neumann entanglement entropy is a physical quantity that measures non-local degrees of freedom. This does not cause any bias in the final calculation. From the perspective of the stabilizer matrix G, the above modifications mean replacing the row corresponding to O_1 with k_O and the rows corresponding to $O_2, ..., O_m$ with $k_{O_1} + k_{O_2}, ..., k_{O_1} + k_{O_m}$ mod 2.

Next, the von Neumann entanglement entropy for a region U can be obtained in the following

way

$$S_U = rank(G_U) - n_U \tag{3.13}$$

where G_U is a matrix by keeping the columns of G that only belongs to region U and n_U is the number of qubits in region U. Here, finding the rank is performed by simplifying the matrix to row reduced echelon form over Z_2. Once we get von Neumann entanglement entropy from the above approach, we can compute S_{topo} and mutual information by restricting U to be any region we are interested in. Finally, we need to average S_{topo} (mutual information) over many realizations as

$$\overline{S_{topo}} = \frac{1}{N} \sum_{i=1}^{N} S_{topo,i} \tag{3.14}$$

where N is the number of realizations we are averaging. We count a full history of the circuit, which contains the locations and types of measurement gates and its measurement outcome at the time step, as one realization. As one can see, this method involving computation with matrices only has a size on the order of L and does not require any renormalization process of the wavefunction $|\Psi\rangle$.

3.4 Results

In this section, we present the results of our simulation. The phase diagram is shown in 3.4. We have one multicritical point and two critical lines. The upper critical line ($P_{XZX} = 0.5$) is mapped out by the computation of topological entanglement entropy. The lower critical line ($P_Z = 0.5$) is mapped out by the computation of mutual information. Even though there is no well-defined Hamilitonian in our system, this phase diagram still has some similarities with 1.1. We have one critical point at $P_{XX} = 0, P_Z = P_{XZX}$ and another one at $P_{XZX} = 0, P_Z = P_{XX}$. These critical points match with $h = \lambda_2 = 1, \lambda_1 = 0$ and $h = \lambda_1 = 1, \lambda_1 = 0$. Critical point A match with $h = 0, \lambda_1 = \lambda_2$. Similarly, $P_{XX} = 0, P_Z = P_{XZX}$ is a multicritical point at which two critical lines meet. However, our tuning parameters represent the probability, which can not go below zero. Thus, we can not obtain the lower half of the phase diagram as 1.1.

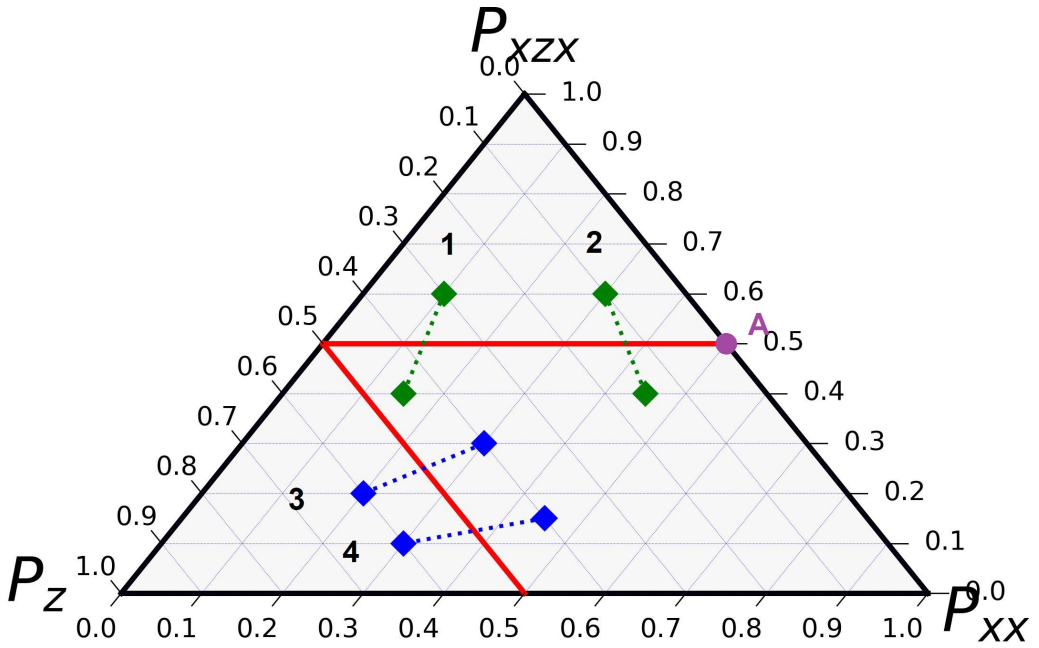

Figure 3.4: A ternary phase diagram. Any point on the phase diagram satisfy $P_Z + P_{XX} + P_{XZX} = 1$. Red solid lines are critical lines. Green lines are paths we take to detect phase transitions by S_{topo}. Blue lines are paths we take to detect phase transitions by mutual information. Point A is a critical point on the line $P_{XZX} + P_{XX} = 1$.

3.4.1 Topological entanglement entropy S_{topo}

In order to probe the upper critical line ($P_{XZX} = 0.5$), we compute topological entanglement entropy along a few paths at different system sizes from the smallest 32 qubits to 256 qubits. The number of realizations we are averaging over depends on the number of qubits. For $L = 32$ and $L = 64$, the number of realizations is 5000. For $L = 128$ and $L = 256$, we only average over 2000 realizations. As we can see from 3.5, 3.6, and 3.7, we certainly see a phase transition happens as we cross the line ($P_{XZX} = 0.5$). At $P_{XZX} > 0.5$, S_{topo} equals some integer values which correspond to the number of boundary modes. At $P_{XZX} < 0.5$, S_{topo} gradually decreases as we go further away from the transition point (becomes strictly zero in thermodynamic limit). Furthermore, we carry out the finite-size scaling and find the critical exponent ν to be around 1.3. The procedure of finite-size scaling is shown below.

3.4.1.1 Finite-size Scaling

To obtain critical exponent ν, we must carry out finite-size scaling [LAB21]. First, we equal our S_{topo} and mutual information to be the following finite-size scaling form.

$$S_{topo}(P, L) = G((P - P_C)L^{1/\nu}) \tag{3.15}$$

$$|I(P, L) - I(P_C, L))| = H((P - P_C)L^{1/\nu}) \tag{3.16}$$

where P_C is the critical probability and $G(...)$,$H(...)$ are some arbitrary functions which depend on dimensionless quantity $(P - P_C)L^{1/\nu}$. Since S_{topo} or mutual information is unitless, no prefactor appears in front of the function G. For a correct choice of ν, all data points should lie on the curve $G((P - P_C)L^{1/\nu})$ when we plot S_{topo} vs $(P - P_C)L^{1/\nu}$. This is achieved by minimizing an objective function with the following form.

$$\epsilon(\nu) = \frac{1}{n-2}\sum_{i=2}^{n-1}(y_i - \overline{y_i})^2 \tag{3.17}$$

where n is the total number of data points, $y_i = S_{topo}(P_i, L_i)$ and $\overline{y_i}$ can be calculated as

$$\overline{y_i} = \frac{(X_{i+1} - X_i)y_{i-1} - (X_{i-1} - X_i)y_{i+1}}{X_{i+1} - X_{i-1}} \tag{3.18}$$

where $X_i = (P_i - P_C)L^{1/\nu}$ with $X_1 < X_2 ... < X_n$.

3.4.2 Mutual information I

To probe the lower critical line ($P_Z = 0.5$), we compute the mutual information along a few paths at different system sizes from the smallest 32 qubits to 256 qubits. The number of realizations we are averaging over is similar to S_{topo} case. As we can see from 3.8 and 3.9, we also see a phase transition happens as we cross the line ($P_Z = 0.5$). At $P_Z > 0.5$, mutual information is non-zero due to long-range entanglement between two ends of the system. At $P_Z < 0.5$, mutual information gradually decreases as we go further away from the transition (becomes strictly zero in thermodynamic limit). Furthermore, we also carry out the finite-size scaling and find the critical exponent ν to be around 1.3.

Additionally, we obtain the dynamical critical exponent z by inspecting the time and spatial dependence of the entanglement entropy at the critical point. In 3.10 top. we see the growth of half-chain entanglement entropy follows the fitting line $S_{L/2}(t) = a_t Log(t) + b$. The form of the fitting function comes from a certain feature of the critical point. Switching to the bottom, we also see how the size of the subsystem affects its entanglement entropy. The fitting line is $S_{L/2} = a_x Log(L/\pi sin(\pi x/L)) + c$. We find out that $a_x = a_t = 0.23$ and thus conclude the dynamical exponent z is one.

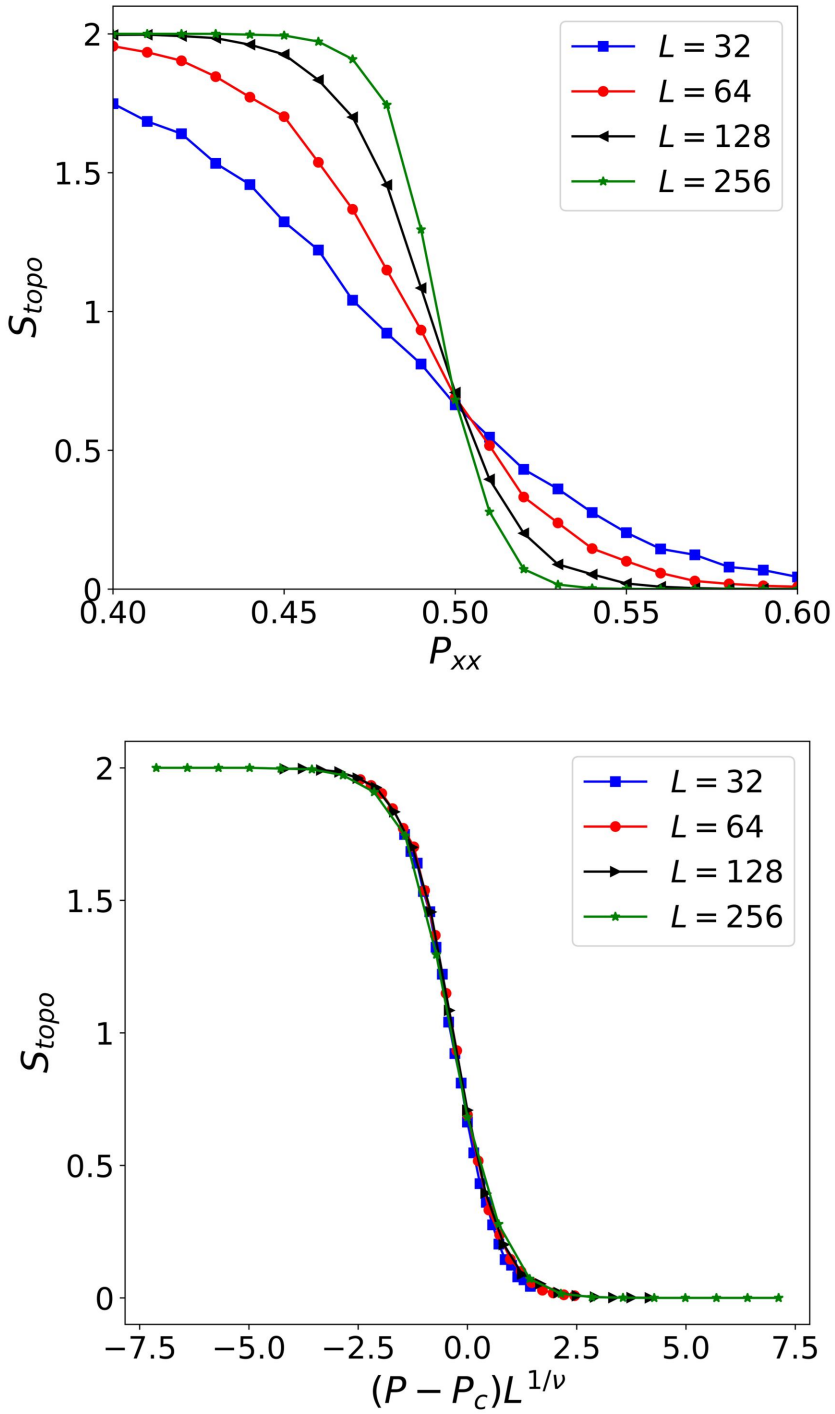

Figure 3.5: Along $P_{XX} + P_{XZX} = 1$. Top: A phase transition occurs at $P_{XX} = 0.5$. In the thermodynamic limit, $S_{topo} = 2$ tells us that there exist two degrees of freedom at the boundary of the chain for $P_{XX} < 0.5$. Bottom: Based on the results of finite size scaling, we see a critical point with critical exponent $\nu = 1.3$.

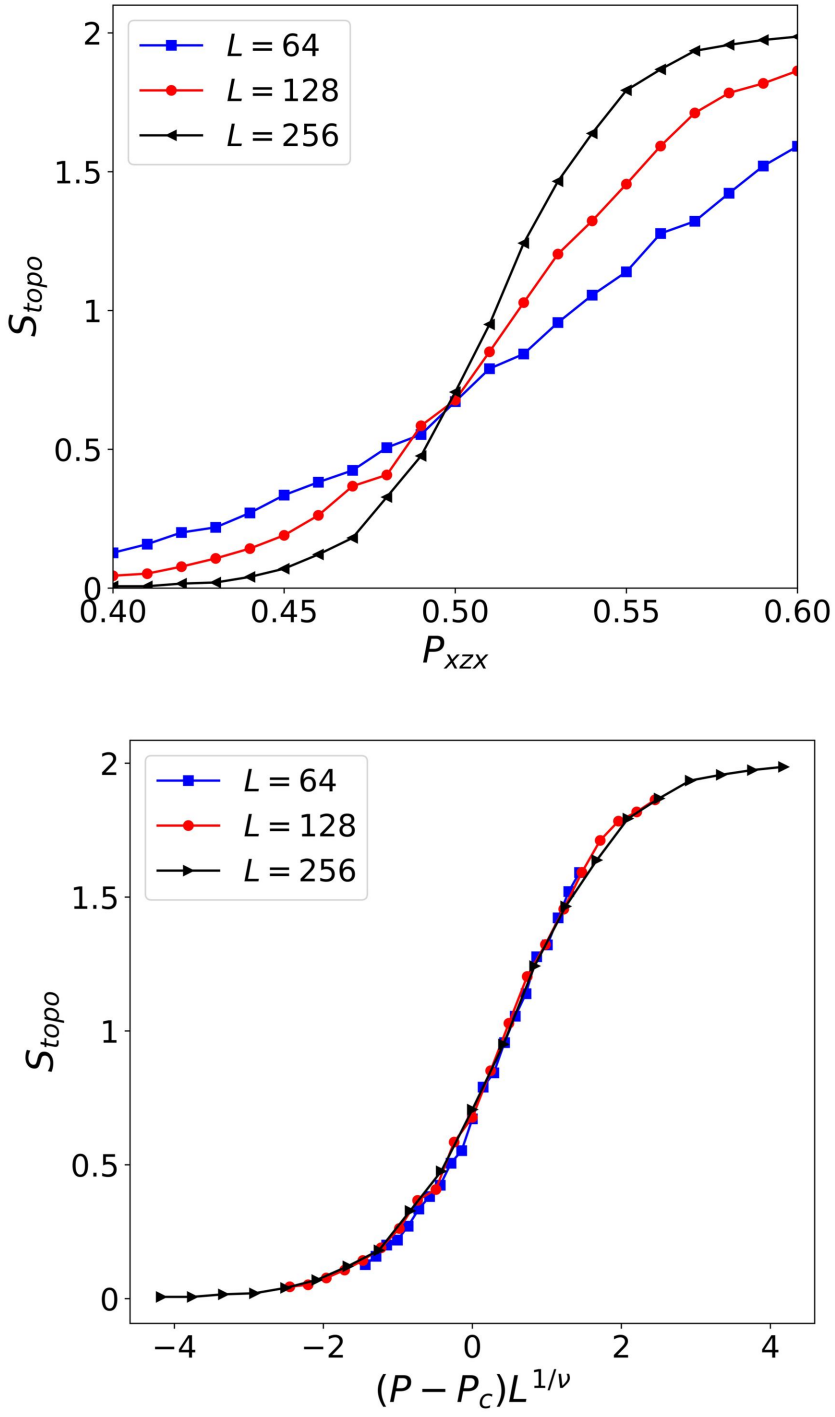

Figure 3.6: Top: Along the path 1 ($P_Z > P_{XX}$) in the phase diagram. Bottom: Finite-size scaling also shows the critical exponent $\nu = 1.3$ along the critical line $P_{XZX} = 0.5$.

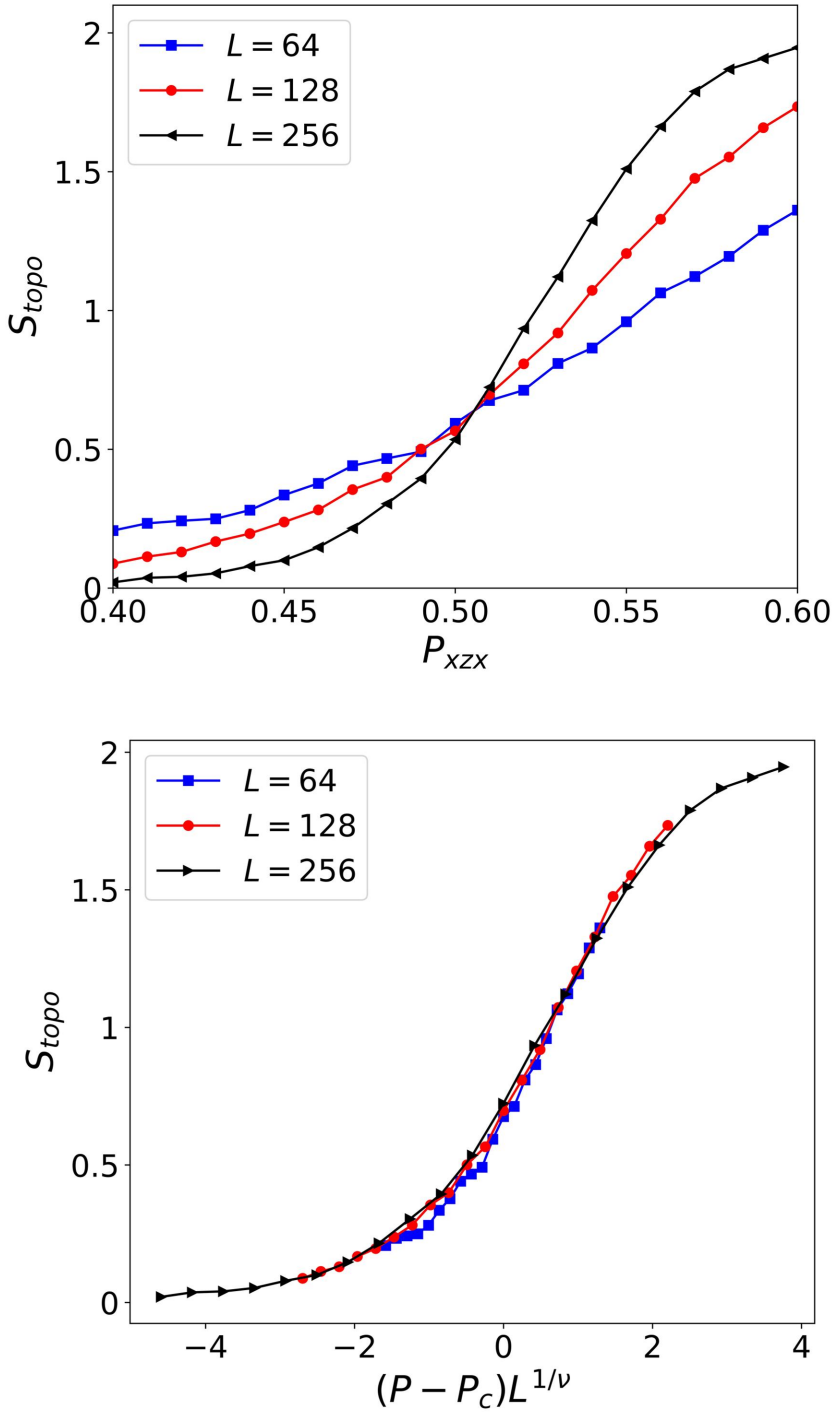

Figure 3.7: Top: Along the path 2 ($P_Z < P_{XX}$) in the phase diagram. Bottom: Finite-size scaling also shows the critical exponent $\nu = 1.3$ along the critical line $P_{XZX} = 0.5$.

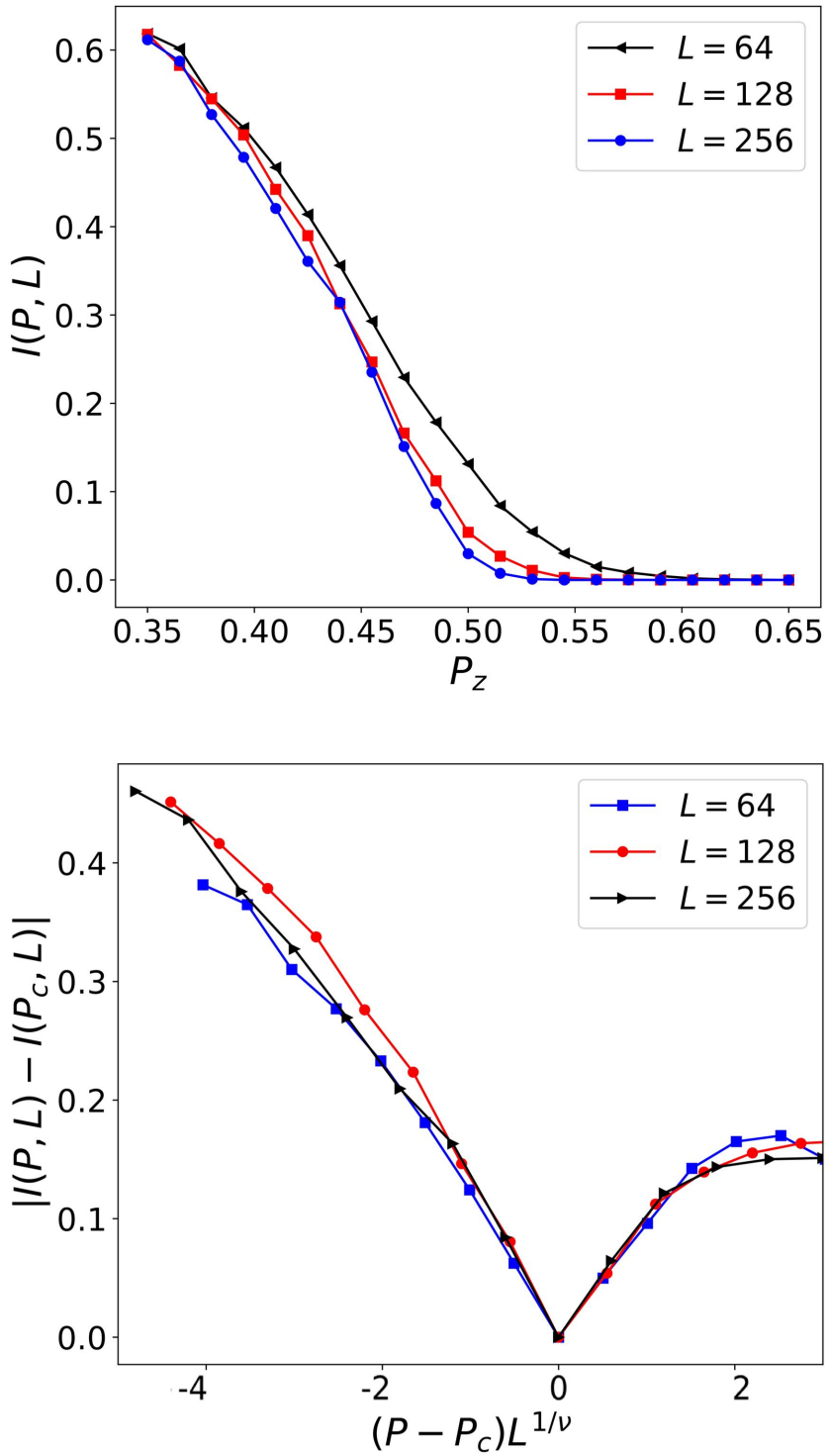

Figure 3.8: Along path 3 $P_{XX} = P_{XZX}$. Top: A phase transition occurs at $P_Z = 0.5$. Bottom: Based on the results of finite size scaling, we have a critical point with critical exponent $\nu = 1.3$.

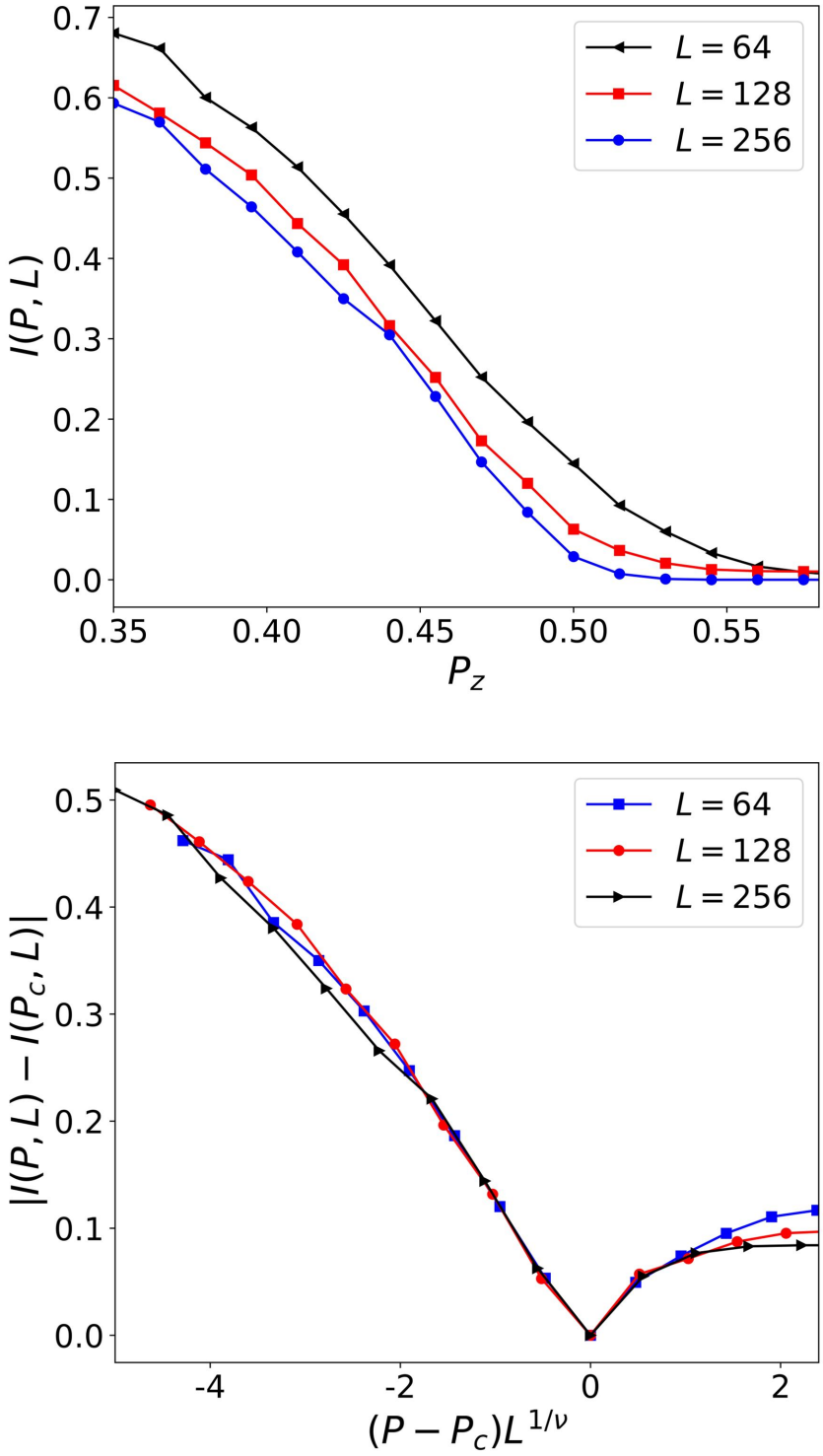

Figure 3.9: Along path 4 $P_{XX} > P_{XZX}$. Top: A phase transition also occurs at $P_Z = 0.5$. Bottom: Based on the results of finite size scaling, we also have a critical point with critical exponent $\nu = 1.3$.

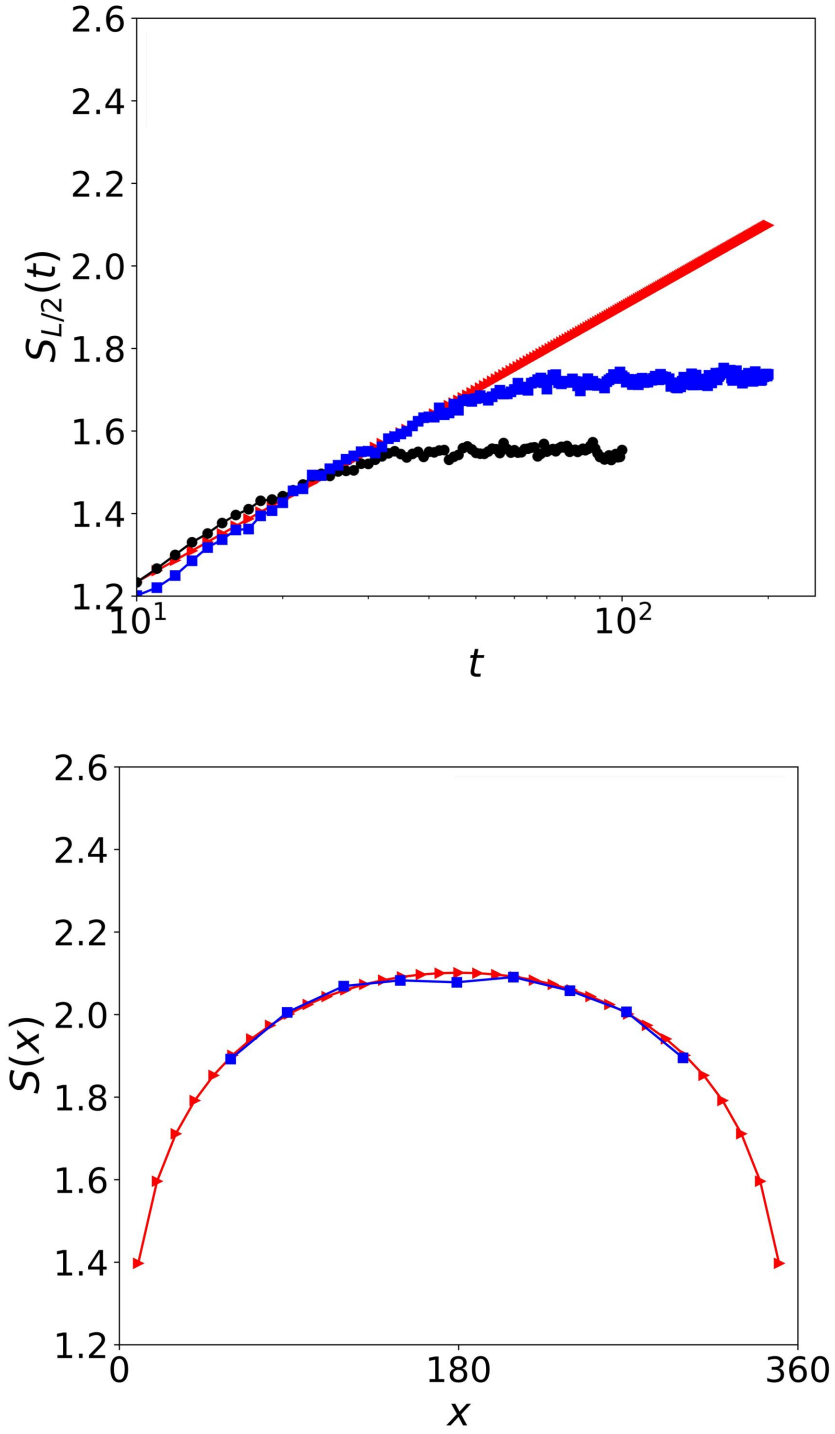

Figure 3.10: At the critical point ($P_{XZX} = 0.5$ and $P_Z = P_{XX}$). Top: half-chain entanglement entropy versus time. Red: logarithmic fitting line. Black: $L = 128$. Blue: $L = 256$. Bottom: entanglement entropy of the subregion vs the length of the subregion at $L = 360$. Red: logarithmic fitting line. Blue: Data.

[AG04] Scott Aaronson and Daniel Gottesman. "Improved simulation of stabilizer circuits." *Physical Review A*, **70**(5):052328, 2004.

[AMR20] Faruk Abdulla, Priyanka Mohan, and Sumathi Rao. "Curvature function renormalization, topological phase transitions, and multicriticality." *Physical Review B*, **102**(23):235129, 2020.

[And58] Philip W Anderson. "Coherent excited states in the theory of superconductivity: Gauge invariance and the Meissner effect." *Physical review*, **110**(4):827, 1958.

[AP17] Dmitry A Abanin and Zlatko Papić. "Recent progress in many-body localization." *Annalen der Physik*, **529**(7):1700169, 2017.

[BM71] Eytan Barouch and Barry M McCoy. "Statistical mechanics of the X y model. II. Spin-correlation functions." *Physical Review A*, **3**(2):786, 1971.

[Car10] Lincoln Carr. *Understanding quantum phase transitions*. CRC press, 2010.

[CBQ20] Soonwon Choi, Yimu Bao, Xiao-Liang Qi, and Ehud Altman. "Quantum error correction in scrambling dynamics and measurement-induced phase transition." *Physical Review Letters*, **125**(3):030505, 2020.

[CHN88] Sudip Chakravarty, Bertrand I Halperin, and David R Nelson. "Low-temperature behavior of two-dimensional quantum antiferromagnets." *Physical review letters*, **60**(11):1057, 1988.

[CHN89] Sudip Chakravarty, Bertrand I Halperin, and David R Nelson. "Two-dimensional quantum Heisenberg antiferromagnet at low temperatures." *Physical Review B*, **39**(4):2344, 1989.

[CNP19] Amos Chan, Rahul M Nandkishore, Michael Pretko, and Graeme Smith. "Unitary-projective entanglement dynamics." *Physical Review B*, **99**(22):224307, 2019.

[Con17] Mucio Continentino. *Quantum scaling in many-body systems*. Cambridge University Press, 2017.

[CSB09] Gang Chen, Andreas P Schnyder, and Leon Balents. "Excitation spectrum and magnetic field effects in a quantum critical spin-orbital system: The case of FeSc 2 S 4." *Physical Review B*, **80**(22):224409, 2009.

[Deu91] Josh M Deutsch. "Quantum statistical mechanics in a closed system." *Physical review a*, **43**(4):2046, 1991.

[DK97] Oleg Derzhko and Taras Krokhmalskii. "Dynamic structure factor of the spin-1 2 transverse Ising chain." *Physical Review B*, **56**(18):11659, 1997.

[EFG15] Jens Eisert, Mathis Friesdorf, and Christian Gogolin. "Quantum many-body systems out of equilibrium." *Nature Physics*, **11**(2):124–130, 2015.

[EYB88] Y Endoh, K Yamada, RJ Birgeneau, DR Gabbe, HP Jenssen, MA Kastner, CJ Peters, PJ Picone, TR Thurston, JM Tranquada, et al. "Static and dynamic spin correlations in pure and doped La 2 CuO 4." *Physical Review B*, **37**(13):7443, 1988.

[GH20] Michael J Gullans and David A Huse. "Dynamical purification phase transition induced by quantum measurements." *Physical Review X*, **10**(4):041020, 2020.

[GKE10] WD Goetze, U Karahasanovic, and FHL Essler. "Low-temperature dynamical structure factor of the two-leg spin-1 2 Heisenberg ladder." *Physical Review B*, **82**(10):104417, 2010.

[Her76] John A Hertz. "Quantum critical phenomena." *Physical Review B*, **14**(3):1165, 1976.

[HNO14] David A Huse, Rahul Nandkishore, and Vadim Oganesyan. "Phenomenology of fully many-body-localized systems." *Physical Review B*, **90**(17):174202, 2014.

[JC06] Xun Jia and Sudip Chakravarty. "Quantum dynamics of an Ising spin chain in a random transverse field." *Physical Review B*, **74**(17):172414, 2006.

[JEK08] AJA James, FHL Essler, and RM Konik. "Finite-temperature dynamical structure factor of alternating Heisenberg chains." *Physical Review B*, **78**(9):094411, 2008.

[JGE09] AJA James, WD Goetze, and FHL Essler. "Finite-temperature dynamical structure factor of the Heisenberg-Ising chain." *Physical Review B*, **79**(21):214408, 2009.

[JYV20] Chao-Ming Jian, Yi-Zhuang You, Romain Vasseur, and Andreas WW Ludwig. "Measurement-induced criticality in random quantum circuits." *Physical Review B*, **101**(10):104302, 2020.

[KC05] Angela Kopp and Sudip Chakravarty. "Criticality in correlated quantum matter." *Nature Physics*, **1**(1):53–56, 2005.

[KFM14] AW Kinross, M Fu, TJ Munsie, HA Dabkowska, GM Luke, Subir Sachdev, and T Imai. "Evolution of quantum fluctuations near the quantum critical point of the transverse field Ising chain system CoNb 2 O 6." *Physical Review X*, **4**(3):031008, 2014.

[Kit01] A Yu Kitaev. "Unpaired Majorana fermions in quantum wires." *Physics-uspekhi*, **44**(10S):131, 2001.

[KKR21] Ranjith R Kumar, YR Kartik, S Rahul, and Sujit Sarkar. "Multi-critical topological transition at quantum criticality." *Scientific Reports*, **11**(1):1004, 2021.

[KP06] Alexei Kitaev and John Preskill. "Topological entanglement entropy." *Physical review letters*, **96**(11):110404, 2006.

[LAB21] Ali Lavasani, Yahya Alavirad, and Maissam Barkeshli. "Measurement-induced topological entanglement transitions in symmetric random quantum circuits." *Nature Physics*, **17**(3):342–347, 2021.

[LB20] Nicolai Lang and Hans Peter Büchler. "Entanglement transition in the projective transverse field Ising model." *Physical Review B*, **102**(9):094204, 2020.

[LCF18] Yaodong Li, Xiao Chen, and Matthew PA Fisher. "Quantum Zeno effect and the many-body entanglement transition." *Physical Review B*, **98**(20):205136, 2018.

[LCF19] Yaodong Li, Xiao Chen, and Matthew PA Fisher. "Measurement-driven entanglement transition in hybrid quantum circuits." *Physical Review B*, **100**(13):134306, 2019.

[LSM61] Elliott Lieb, Theodore Schultz, and Daniel Mattis. "Two soluble models of an antiferromagnetic chain." *Annals of Physics*, **16**(3):407–466, 1961.

[MAG14] CM Morris, R Valdés Aguilar, A Ghosh, SM Koohpayeh, J Krizan, RJ Cava, O Tchernyshyov, TM McQueen, and NP Armitage. "Hierarchy of bound states in the one-dimensional ferromagnetic Ising chain CoNb 2 O 6 investigated by high-resolution time-domain terahertz spectroscopy." *Physical review letters*, **112**(13):137403, 2014.

[NCH12] Yuezhen Niu, Suk Bum Chung, Chen-Hsuan Hsu, Ipsita Mandal, S Raghu, and Sudip Chakravarty. "Majorana zero modes in a quantum Ising chain with longer-ranged interactions." *Physical Review B*, **85**(3):035110, 2012.

[NF93] AH Castro Neto and Eduardo Fradkin. "The thermodynamics of quantum systems and generalizations of Zamolodchikov's C-theorem." *Nuclear Physics B*, **400**(1-3):525–546, 1993.

[NNZ22] Crystal Noel, Pradeep Niroula, Daiwei Zhu, Andrew Risinger, Laird Egan, Debopriyo Biswas, Marko Cetina, Alexey V Gorshkov, Michael J Gullans, David A Huse, et al. "Measurement-induced quantum phases realized in a trapped-ion quantum computer." *Nature Physics*, **18**(7):760–764, 2022.

[Pes18] Michael Peskin. *An introduction to quantum field theory*. CRC press, 2018.

[Pfe70] Pierre Pfeuty. "The one-dimensional Ising model with a transverse field." *ANNALS of Physics*, **57**(1):79–90, 1970.

[Pre18] John Preskill. "Quantum computing in the NISQ era and beyond." *Quantum*, **2**:79, 2018.

[PTV07] William H Press, Saul A Teukolsky, William T Vetterling, and Brian P Flannery. *Numerical recipes 3rd edition: The art of scientific computing*. Cambridge university press, 2007.

[RDO08] Marcos Rigol, Vanja Dunjko, and Maxim Olshanii. "Thermalization and its mechanism for generic isolated quantum systems." *Nature*, **452**(7189):854–858, 2008.

[Sac99] Subir Sachdev. "Quantum phase transitions." *Physics world*, **12**(4):33, 1999.

[Sar17] Sujit Sarkar. "Topological quantum phase transition and local topological order in a strongly interacting light-matter system." *Scientific Reports*, **7**(1):1–15, 2017.

[Sar18] Sujit Sarkar. "Quantization of geometric phase with integer and fractional topological characterization in a quantum ising chain with long-range interaction." *Scientific reports*, **8**(1):5864, 2018.

[SGC97] Shivaji Lal Sondhi, SM Girvin, JP Carini, and Dan Shahar. "Continuous quantum phase transitions." *Reviews of modern physics*, **69**(1):315, 1997.

[SH21] Shengqi Sang and Timothy H Hsieh. "Measurement-protected quantum phases." *Physical Review Research*, **3**(2):023200, 2021.

[SPA13] Maksym Serbyn, Zlatko Papić, and Dmitry A Abanin. "Local conservation laws and the structure of the many-body localized states." *Physical review letters*, **111**(12):127201, 2013.

[Sre94] Mark Srednicki. "Chaos and quantum thermalization." *Physical review e*, **50**(2):888, 1994.

[SRN19a] Brian Skinner, Jonathan Ruhman, and Adam Nahum. "Measurement-induced phase transitions in the dynamics of entanglement." *Physical Review X*, **9**(3):031009, 2019.

[SRN19b] Brian Skinner, Jonathan Ruhman, and Adam Nahum. "Measurement-induced phase transitions in the dynamics of entanglement." *Physical Review X*, **9**(3):031009, 2019.

[SRS19] Marcin Szyniszewski, Alessandro Romito, and Henning Schomerus. "Entanglement transition from variable-strength weak measurements." *Physical Review B*, **100**(6):064204, 2019.

[YC] Hui Yu and Sudip Chakravarty. "Quantum critical fan arising from critical lines at finite temperatures." *In preparation*.

[YC23] Hui Yu and Sudip Chakravarty. "Quantum critical points, lines, and surfaces." *Physical Review B*, **107**(4):045124, 2023.

[You97] AP Young. "Finite-temperature and dynamical properties of the random transverse-field Ising spin chain." *Physical Review B*, **56**(18):11691, 1997.

[ZLS15] Jan Zaanen, Yan Liu, Ya-Wen Sun, and Koenraad Schalm. *Holographic duality in condensed matter physics*. Cambridge University Press, 2015.